Genetic screening for single-cell variability modulators driving therapy resistance

Eduardo A. Torre[1], Eri Arai[3,*], Sareh Bayatpour[2,*], Lauren E. Beck[2], Benjamin L. Emert[6], Sydney M. Shaffer[2,5], Ian A. Mellis[6], Krista A. Budinich[3], Ashani Weeraratna[4], Junwei Shi[3,**], Arjun Raj[2,3,7,**]

[1] Biochemistry and Molecular Biophysics Graduate Group, Perelman School of Medicine, University of Pennsylvania, Philadelphia, PA
[2] Department of Bioengineering, School of Engineering and Applied Science, University of Pennsylvania, Philadelphia, PA
[3] Department of Cancer Biology, Perelman School of Medicine, University of Pennsylvania, Philadelphia, PA
[4] The Wistar Institute, Philadelphia, PA
[5] Department of Pathology and Laboratory Medicine, Perelman School of Medicine, University of Pennsylvania, Philadelphia, PA
[6] Genomics and Computational Biology Graduate Group, Perelman School of Medicine, University of Pennsylvania, Philadelphia, PA
[7] Department of Genetics, Perelman School of Medicine, University of Pennsylvania, Philadelphia, PA
*Equal contribution
**Co-corresponding authors

Abstract:

Cellular plasticity describes the ability of cells to transition from one set of phenotypes to another. In the context of cancer therapeutics, plasticity refers to transient fluctuations in the molecular state of tumor cells, driving the formation of rare cells that can survive drug treatment and ultimately reprogram into a stably resistant fate. However, the biological processes governing this cellular plasticity remain unknown. We used CRISPR/Cas9 genetic screens to reveal genes that affect cell fate decisions by altering cellular plasticity. We discovered a mode of altering resistance based on cellular plasticity that, contrary to known mechanisms, pushes cells towards a more differentiated state. The interaction of this pathway with therapy resistance has a temporal dependence, requiring inhibition specifically before the addition of the main therapy in order to exert an effect on cell fate, i.e., therapy resistance. Together, our results indicate that identifying pathways modulating cellular plasticity has the potential to alter cell fate decisions and may provide a new avenue for treating drug resistance.

Introduction

Plasticity is often used to describe the ability of cells to transition from one phenotype to another, at times enabling cells to adapt and survive in the face of a variety of stimuli and challenges, for instance, in regeneration, wound healing, and the induction of pluripotency. Plasticity itself can typically be decomposed into a stimulus-independent and dependent phase. The first phase typically consists of individual, often rare, cells within the population being “primed” for the cell fate transition. Then, upon the stimulus, these primed cells are selectively reprogrammed to adopt the new phenotype. Thus, a major question in single cell biology has

been determining the molecular differences specific to these rare primed cells ("cell states") before a stimulus and connecting those states to their ultimate phenotype ("cell fates") after the stimulus reprograms them. Recently, a number of studies have developed the link between states and fates that underlies plasticity in a number of contexts (*1–8*). However, to date, little is known about the pathways that can manipulate the fluctuations that drive the priming of these rare cellular states and thus their subsequent fates, leaving their molecular basis and potential for therapeutic application largely unrealized.

Therapy resistance in melanoma is an excellent example of cellular plasticity (*9*, *10*). Therapies such as vemurafenib designed to inhibit particular oncogenic targets can often kill most of the tumor cells, but a few remaining cells can continue to proliferate, ultimately repopulating the tumor. While the mechanisms underlying this therapy resistance can sometimes be the result of a genetic mutation, many recent studies, both in melanoma and other cancers, suggest that cellular plasticity may also dictate which cells are able to survive drug treatment, with rare primed cells being reprogrammed by the addition of drug into a stably resistant state (*8*, *11–21*). In melanoma, this rare primed cellular state, which we refer to as the pre-resistant cellular state, is often marked by transiently high expression of several resistance marker genes, such as *EGFR*, *NGFR* and *AXL* (Fig. 1A, top). Once these cells are exposed to drug, they are are reprogrammed into a new cellular fate in which the transient pre-resistant phenotype is converted to a stably drug-resistant phenotype characterized by massive changes in signaling and gene expression profiles. This paradigm of resistance has a number of critical differences from the more conventional model of mutational causes of drug resistance—notably, while genetic mutations largely arise through spontaneous, stochastic processes, non-genetic fluctuations that drive the primed cellular states can in principle occur due to the changes in activity of specific biological pathways. Targeting these pathways specifically could have the potential to enhance or inhibit the formation of cells in the primed state independent of the addition of drug. We were thus interested in dissecting the molecular regulators of cellular state and how those might consequently affect the ultimate drug-resistant fates that cells can adopt.

With the advent of CRISPR/Cas9 technology, it is now possible to perform genetic screens to identify regulators of various molecular processes. For most cell fate transitions, including therapy resistance, virtually all screens have been designed to detect changes to the ultimate cellular fate only—i.e., changes in the final number of resistant cells, typically measured as a proliferation phenotype (*22–25*). However, an important aspect of plasticity is the process of stimulus-independent priming of rare cells in the population, which in this context is represented by the transient fluctuations in single cells that lead to cellular states that ultimately reprogram into a stably resistant cell fate (*14*). This priming processes may in principle have distinct regulatory mechanisms to that of the acquisition of resistance as a whole, presenting an opportunity to leverage screening techniques to specifically identify factors affecting cellular state before the addition of drug (Fig. 1A, middle). These factors may then also affect the overall degree of drug resistance, but potentially through new, previously undiscovered mechanisms that allow for new therapeutic targets that affect drug resistance in ways not revealed by classical resistance screens.

We here describe the results of genetic screens designed to capture modulators of single cell state variability that subsequently affect cell fate decisions. Specifically, in the context of melanoma, we performed pooled CRISPR/Cas9 genetic screens to reveal modulators of the rare cell state that drives drug resistance. This new type of screen revealed several new factors that affect both cellular state and ultimate fate. The transcriptome profiles induced by knocking out these factors revealed a novel mechanism that can increase or reduce drug resistance by increasing or decreasing the activity of differentiation pathways, respectively, as opposed to the more typical increased drug resistance induced by decreased differentiation. Drugs targeting these new mechanisms display a variety of synergistic effects when coupled with therapy, which can be dependent on the relative timing of drug application. Together, our results indicate that modulating cellular plasticity can alter cell fate decisions and may provide a new avenue for treating drug resistance.

Results

CRISPR/Cas9 genetic screens identify factors that affect cellular states

We wanted to identify factors that affected the fluctuations in cellular state that lead to single cells being resistant to drug. We took advantage of a clonal melanoma cell line (WM989 A6-G3) that we have extensively characterized as exhibiting resistance behavior in cell culture that is broadly comparable to that displayed in patients (*14*, *21*, *26*). Phenomenologically, in cell culture, we observe that upon addition of a roughly cytostatic dose of the $BRAF^{V600E}$ inhibitor vemurafenib (1μM), the vast majority of cells die or stop growing, but around 1 in 2,000-3,000 cells continues to proliferate, ultimately forming a resistant colony after 2-3 weeks in culture in vemurafenib. We have previously demonstrated that before the application of drug, there is a rare subpopulation of cells (pre-resistant cells) that express high levels of a number of markers, and that these cells are far more likely to be resistant than other cells (*14*). In order to identify modulators of the fluctuations that lead to the formation of this subpopulation of pre-resistant cells, we designed a large scale loss-of-function pooled CRISPR genetic screen (which we dubbed the “state screen”) comprised of ~13,000 single guide RNAs (sgRNAs) targeting functionally relevant domains of ~2,000 proteins, with roughly six distinct single guide RNAs per domain (1402 transcription factor targets, 481 kinase targets, 176 epigenetic targets; each single guide RNA targets an important functional domain, see Supplemental Tables 1-3) (*27–29*). To conduct the screen, we stably integrated *Streptococcus pyogenes* Cas9 (spCas9) into the WM989-A6-G3 cell line, creating the clonal line WM989-A6-G3-Cas9-5a3.
Our screening strategy consisted of first transducing the pooled library of single guide RNAs into a population of cells using lentivirus at a low multiplicity of infection. Given that pre-resistant cells show up only rarely within the population, we needed to ensure that we had sufficient cell numbers in order to effectively sample differences in the frequency of pre-resistant cells. Thus

we expanded the culture to maintain around 50,000-250,000 total cells per each individual single guide RNA, for a total of roughly a billion cells. We then used a combination of magnetic sorting and flow cytometry to isolate cells that were positive for both EGFR and NGFR expression, both of which are prominent markers of the pre-resistant rare cell subpopulation. We then sequenced the single guide RNAs in this sorted subpopulation to determine which single guide RNAs were over- or under-represented as compared to the unsorted total population. Here, over-representation suggests that knockout of the gene leads to an increased frequency of $NGFR^{HIGH}/EGFR^{HIGH}$ cells and vice versa (Fig. 1B). To select "hits" from the screen, we designed a series of criteria to identify and rank targets into confidence tiers (see methods for a detailed description of the selection criteria). For ranking targets, we considered a target in the screen to be a high confidence "hit" if we detected a two-fold change in abundance for ≥ 75% (Tier 1) or ≥ 66% (Tier 2) of the single guide RNAs. We considered targets with a two-fold change in ≥ 50% (Tier 3) or < 50% (Tier 4) of its single guide RNAs to be lower confidence hits.

By these criteria, we obtained a set of 61 high confidence targets identified as factors affecting the frequency of $NGFR^{HIGH}/EGFR^{HIGH}$ cells in our screen (Fig. 1C, Supplemental Table 4). Of these, 25 increased the frequency of $NGFR^{HIGH}/EGFR^{HIGH}$ cells, while the remaining 36 decreased the frequency. Beyond known factors in melanoma biology such as *SOX10* and *MITF* (*26*, *30*–*32*), we identified several new factors not previously known to affect resistance to $BRAF^{V600E}$ inhibition. These include *DOT1L*, which encodes an H3K79 methyltransferase associated with melanoma oncogenesis (*33*), and *BRD2*, which encodes a protein that is a member of the BET family, often overexpressed in human melanoma (*34*). To assess the robustness and generality of our results, we performed a secondary targeted screen using 86 of the targets identified by our first screen, of which 34 were high confidence hits (Supplemental Fig. 2, Supplemental Table 4). We found that 25/34 targets replicated in the original WM989-A6-G3-Cas9 line and 20/34 replicated in another melanoma line (451Lu-Cas9). Also, we observed qualitative agreement for most of the lower confidence hits as well, suggesting that there may be several other factors affecting pre-resistance that our screen was not powerful enough to detect.

A cell survival "fate" screen reveals a different set of factors that modulate drug resistance

Our variability "state" screen is conceptually distinct from more conventional resistance screen designs in which the screened phenotype is overall survival and proliferation in the face of drug. Our hypothesis was that those more conventional screens would identify a different set of factors because the underlying biological processes may be different. To test this hypothesis, we also performed a parallel, conventional genetic screen for resistance to find modulators that specifically altered cellular "fate"; i.e., formation of resistant colonies when exposed to $BRAF^{V600E}$ inhibition. Here, we used the same cells and the same library of single guide RNAs, but instead of isolating $NGFR^{HIGH}/EGFR^{HIGH}$ cells, we added vemurafenib and grew the cells until large resistant colonies formed, at which point we isolated DNA and sequenced it to look for over- and

under-represented single guide RNAs as before (Supplemental Fig. 3A). Here, if a single guide RNA is overrepresented in the resistant cell population, it means that knocking out the gene it targets resulted in an increase in the number of cells that survive the drug and acquire resistance, and vice versa for under-representation of single guide RNAs.

This fate screen identified 24 high confidence factors (Supplemental Fig. 3B, Supplemental Table 4). Among those, there were a number of factors that affect or act downstream of signaling pathways such as MAPK (CSK) (*35*), Wnt/B-catenin (*KDM2A*)(*36*), and Hippo (*LATS2*) (*37*). 20 of the 24 were predicted to enhance the number of resistant cells, while the remaining 4 were predicted to decrease the number of resistant cells. 5 of the hits were also identified by our state screen (Fig. 1D). As with the previous screen, we performed a secondary targeted screen in both this line and another melanoma cell line, with 7/9 factors showing similar effects (Supplemental Fig. 4, Supplemental Table 4).

The lack of correspondence between the two screens most likely reflects the fact that distinct biological processes may play a more dominant role in either single cell variability or other aspects of the overall acquisition of resistance. If it were possible to run the screen for overall acquired resistance to saturation—i.e., isolate *all possible* factors affecting resistance—then we would in principle be able to find all variability factors that affected the resistance phenotype as well in that single screen. However, bottlenecks in the screening process owing to the rarity of the resistance phenotype at the single cell level meant that some factors (e.g. *CSK*) may come to dominate the fate screen, making it difficult to fully capture all factors through just the conventional resistance screen alone.

Factors affecting variability also affect overall drug resistance to different degrees

We designed our state screen to identify factors that increase or decrease the percentage of $NGFR^{HIGH}/EGFR^{HIGH}$ cells. The implicit assumption was that increasing the percentage of $NGFR^{HIGH}/EGFR^{HIGH}$ cells would be associated with an increase in the number of cells that went on to acquire drug resistance. However, EGFR and NGFR are, in this context, just markers of the pre-resistant state, and most of the factors identified in the state screen did not appear in our fate screen for factors affecting overall resistance. Thus, it was conceivable that factors identified from our screen might simply affect the transcriptional regulation of these genes but not affect the frequency of cells being in the pre-resistant state *per se*. Thus, we conducted further experiments to demonstrate that: 1. the factors identified actually did change the frequency of cells expressing NGFR as predicted by the screen, and then 2. that these changes in the frequency of $NGFR^{HIGH}$ cells translated into changes in the number of resistant colonies upon application of vemurafenib.

We used immunofluorescence to verify, on 83 targets individually, that knocking out the target led to the predicted increase or decrease in the frequency of $NGFR^{HIGH}$ cells. We found that

most high confidence targets (21/34) and even several low confidence targets (21/49) changed this frequency by at least 50%, with the latter suggesting the existence of further hits our screen did not detect (Fig. 2A; Supplemental Fig. 5A).

We then wanted to test whether these differences in the frequency of $NGFR^{HIGH}$ cells would translate to differences in the number of resistant colonies. We took a subset of these knockout populations (33 different targets, 21 of which were high confidence hits from the state screen), added vemurafenib, and counted the number of resistant colonies after three weeks in drug. We found that 15 of the 21 high confidence hits showed an increase or decrease in the number of resistant colonies that was consistent with the change in the frequency of $NGFR^{HIGH}$ cells, even though only 5 of the 21 hits were high confidence hits in the "fate" screen (Fig. 2B; Supplemental Fig. 5B, left panel). (We also tested seven high confidence targets from the initital fate screen, six of which led to a change in the number of colonies resistant to vemurafenib (Supplemental Fig. 5B, right panel; Supplemental Fig. 6)). Additionally, we used a small molecule inhibitor for DOT1L at non-cytotoxic doses to confirm that inhibition of this target led to dramatic changes in the number of colonies able to survive and proliferate upon $BRAF^{V600E}$ inhibition (Supplemental Fig. 7A-B). Furthermore, DOT1L inhibition led to an increase in the number of resistant colonies not only upon targeting $BRAF^{V600E}$, but also upon MEK inhibition and simultaneous MEK and $BRAF^{V600E}$ inhibition (Supplemental Fig. 7C).

If the level of *NGFR* expression perfectly reflected the probability of a cell becoming resistant upon addition of drug, then changes in the number of resistant colonies should be directly proportional to changes in the number of $NGFR^{HIGH}$ cells. However, while the general trend indicated such a pattern, knockouts of individual genes varied widely in the degree to which this relationship held (Fig. 2B). For instance, knockout of *EP300* resulted in a ~two-fold increase in the number of $NGFR^{HIGH}$ cells but only a small increase in the number of resistant colonies, while knockout of *CSK* resulted in only a small increase in the number of $NGFR^{HIGH}$ but had at least a six-fold increase in the number of resistant colonies. (Importantly, the number of colonies for the CSK knockout is an underestimate due to difficulties in accurately counting colonies in highly-confluent plates, see Supplemental Fig. 5C for raw image of colonies.) This is most likely why CSK was a dominant hit in our screen for full resistance for vemurafenib. Conceptually, a change in the number of resistant colonies without a proportional change in the number of $NGFR^{HIGH}$ cells could result from a change in the mapping between state and fate induced by the drug (perhaps best thought of as a change in "threshold"), or from a shift in the distribution of the internal state of the cells that is not reflected in a change in NGFR expression. While our results cannot conclusive resolve this difference, some of our results argue in favor of changes to the mapping between state and fate itself. For instance, the *CSK* knockout cell line showed an increase in the number of resistant colonies but also an increase in the number of resistant cells that do not form colonies (Supplemental Fig. 5C). This suggested that, in addition to the usual pre-resistant cells that form colonies, an additional set of cells in the *CSK* knockout line were now enabled to survive drug. This suggests that the "threshold" for cells to survive drug may have changed; i.e., the state-fate mapping itself has been altered by the removal of *CSK*.

Relative timing of targeting variability can affect drug resistance

Our two screens, one for variability in cellular state (pre-resistance) and the other for the ultimate cellular fate (stable drug resistance), identified different factors. It is possible that these factors act via distinct mechanisms, and that these mechanisms may potentially interact or override each other in complex ways dependent on relative timing. For instance, a factor identified by our state screen could affect the number of cells in the pre-resistant state, but once cells are subjected to before $BRAF^{V600E}$ inhibition and begin reprogramming, the factor may no longer have any effect. In such a case, inhibiting this factor *before* the adding the $BRAF^{V600E}$ inhibitor would be critical.

To test for such a possibility, we used the DOT1L inhibitor pimenostat (*38*, *39*) (which increases the number of colonies resistant to vemurafenib over a range of doses; Supplemental Fig. 7A) to see if timing of DOT1L inhibition would affect the formation of resistant colonies. In addition to the standard vemurafenib treatment, we both pre-treated with the DOT1L inhibitor for seven days before adding vemurafenib and co-treated with the DOT1L inhibitor concurrently with vemurafenib (we tested both pre-treatment followed by vemurafenib alone and pre-treatment followed by concurrent treatment) (Fig. 2C). We found that pre-inhibition of DOT1L resulted in three-fold more colonies than with $BRAF^{V600E}$ inhibition alone, but that co-treatment with the DOT1L and $BRAF^{V600E}$ inhibitors led to no change in the number of resistant colonies (Fig. 2D), suggesting that DOT1L inhibition is altering the distribution of states of the cells, and consequently the number of cells that develop resistance to $BRAF^{V600E}$ inhibition. Our results demonstrate that the relative timing of inhibition of different pathways can have a profound effect on resistance.

Transcriptomics reveals multiple mechanisms for cellular state and fate modulation

Our screens revealed a large number of factors affecting pre-resistance and full resistance (state and fate) that act across a range of biological processes, including a variety of signaling pathways and transcriptional regulatory mechanisms. Interestingly, *a priori*, no particular pathway appeared to dominate the set of identified factors; however it is possible that seemingly unrelated genes nevertheless affect pre-resistance and resistance through common biological processes.

To look for such pathways, we used RNA sequencing to measure genome-wide transcript abundance levels for 266 knockout cell lines targeting 80 different proteins taken from both screens (each targeted with 2-3 separate single guide RNAs; see supplementary table 4). Of the 80 protein targets, 45 changed the frequency of $NGFR^{HIGH}$ cells by immunofluorescence and/or changed the number of resistant colonies upon adding vemurafenib (Supplemental Figs. 5A-B, 8, and 9).

Initially, we clustered the transcriptome profiles from the different cell lines, including only genes differentially expressed in at least one sample (Supplemental Fig. 10). We found that while the transcriptomes induced by some gene knockouts were clearly distinct (such as *MITF*, *SOX10* and *KDM1A*), many others appeared to show only relatively small differences from the parental cell line, despite the fact that our validation results showed that these knockouts exhibited clear effects on the resistance potential of the population. We thus reasoned that while the sets of genes whose expression change in our knockouts may be non-overlapping, these genes could still belong to similar categories of biological processes; i.e., different knockouts may all affect different genes all within a common pathway, for instance differentiation. Thus, using the transcriptome of each knockout, we performed a gene set enrichment analysis (GSEA, see methods) and obtained an enrichment score for a number of biological processes from the Gene Ontology terms database (Fig. 3A) (*40*). Using these enrichment scores, the knockout lines clustered in a more obvious pattern. Notable clusters include cluster 5, containing the canonical melanocyte master regulators *MITF* and *SOX10*, and cluster 1, containing *DOT1L*, *LATS2*, *RUNX3* and *GATA4*.

Interestingly, knocking out MITF and SOX10 increases drug resistance, as does knocking out most members of cluster 1, but the transcriptome profiles of these two clusters appeared to be roughly opposite of each other. We inspected the GO gene sets in Group E, which appeared maximally different between MITF/SOX10 and cluster 5, and found that these gene sets included several related to differentiation, including sets for melanocyte differentiation and neural crest differentiation (Fig. 3B). The knockout of MITF and SOX10 appeared to decrease the expression of these genes, matching the general consensus that drug resistance is typically driven by dedifferentiation (*8*, *26*). In that context, the finding that most elements of cluster 1 increased resistance by further promoting differentiation was unexpected (Fig. 3C), suggesting a possible novel mechanism by which one could affect drug resistance; the latter has further support from our findings using the DOT1L inhibitor (Fig. 2C). This axis of differentiation was coordinated across several gene sets, as revealed by principal components analysis of the expression heat map (Supplemental Fig. 10B). (Note that the role of *MITF* in therapy resistance in general is complex (*41*)).

Clusters of targets that lead to different degrees of differentiation also seem to correspond to distinct phenotypic profiles, meaning the resultant changes in the frequency of $NGFR^{HIGH}$ cells and number of resistant colonies. For instance, the transcriptomes of the knockouts in cluster 1 seem to mimic many aspects of the transcriptomes of $NGFR^{HIGH}$, $EGFR^{HIGH}$, $NGFR^{HIGH}/EGFR^{HIGH}$, and even vemurafenib resistant melanoma cells (e.g. high expression of genes involved in cell-matrix adhesion, angiogenesis, and cell migration; Fig. 3A,B). Knockout of these targets showed a strong correspondence between the frequency of $NGFR^{HIGH}$ cells and the number of colonies that developed under BRAF inhibition, suggesting that the increase/decrease in the frequency of pre-resistant cells was the cause of increased/decreased resistance (Fig. 3D). Often, this relationship was relatively proportional, as was the case for the knockout of *LATS2, JUNB, FOSL1,* and *CBFB*. For *MITF* and *SOX10* (cluster 5), however, the

relationship between the frequency of NGFR^{HIGH} cells and the number of resistant colonies was much weaker, with very large changes in the latter but not the former. Accordingly, our transcriptomic analysis suggests that these knockouts lead to changes in gene expression that are distinct from those of NGFR^{HIGH}/EGFR^{HIGH} cells.

The transcriptome analysis also revealed different categories of knockouts that resulted in a *reduction* (as opposed to increase) of the number of resistant colonies. Some resistance reducing knockouts (*BRD8* and *PRKAA1*) clustered with *DOT1L*, while another (*BRD2)* clustered with *MITF/SOX10*. It is possible that these factors work in inverse ways to reduce drug resistance by either affecting differentiation or dedifferentiation. Meanwhile, the majority of resistance reducing knockouts appeared to cluster separately into distinct clusters, generally through changes in the expression of a distinct set of genes. For one cluster (cluster 2), the set of genes whose expression was affected included several associated with metabolism (e.g. biosynthesis of amino acids and Acyl Co-A metabolism), suggesting that modulation of metabolic processes may be a means of reducing drug resistance (Supplemental Table 6). The other clusters did not show any coherent set of biological processes affected (e.g. *SRC*, *IRF7*, *PKN2*, among others), rendering that particular pathway or set of pathways rather mysterious.

Discussion

We have here demonstrated, using high-throughput genetic screening, that there are genetic factors that can alter cellular plasticity in cancer cells, thereby affecting their resistance to targeted therapeutics. We identified a variety of new factors that appear to work through new pathways that can affect therapy resistance in novel, time-dependent ways. These factors revealed new possible vulnerabilities that a conventional genetic screen targeting resistance did not uncover, thus demonstrating the potential for screens specifically designed to target single cell variability to reveal new biological mechanisms that may subsequently emerge as therapeutic opportunities. Drug screens targeting gene expression “noise” have also shown similar therapeutic potential (*42*).

While we isolated several new factors that specifically affected cellular variability, it is important to note that no single factor we isolated resulted in a change in cellular variability that was stronger than all the rest; i.e., no factor emerged as the “smoking gun”. This may be the result of the fact that our screen did not target all potential regulators. Alternatively, it may be that the biology of cellular variability is intrinsically multifactorial, with the coherent activity of many factors being required for cells to ultimately enter the highly deviated cellular state responsible for phenotypes like drug resistance (*15*). Larger scale screens may help reveal a more complete picture of the origins of rare cell behavior; however, the limitations imposed by the rarity of the pre-resistant cellular phenotype make this rather difficult. The raw numbers of cells required to properly sample these rare cell behaviors in a pooled genetic screening format remains a major technical challenge for the field of rare cell biology.

Indeed, it is the very difficulty of performing these screens at full depth that provides motivation for screening for variability rather than simply screening for resistance. If one is primarily interested in factors affecting resistance, then in principle such a screen, if carried to saturation, would reveal all such factors, including those that exert such an effect via modulation of cellular variability. However, the degree of overlap in the factors identified between our variability screen and our conventional resistance screen was relatively small. This lack of overlap suggests that distinct biological processes may dominate the results of these differently designed screens. That of course in turn raises the question of why one might want to perform variability screens at all, given that the phenotype of interest is resistance. Our results on timing of variability inhibition suggest that while the mechanisms governing rare cell variability may not appear as potent as those revealed by conventional resistance screens, the fact that they represent *distinct* mechanisms means that they may present an opportunity to be used in tandem. It is also possible that these mechanisms may be more dominant in other, more clinically relevant contexts.

In our validation studies, for several factors, we measured the effects of knocking out those factors on both the number of $NGFR^{HIGH}$ cells (which serves as a proxy for cellular state) and number of resistant colonies upon adding vemurafenib (which is our measurement for cellular fate). Interestingly, different knockouts affected both of these validation metrics differently, with some (e.g. *LATS2*) both increasing the frequency of $NGFR^{HIGH}$ cells as well as concomitantly increasing the number of resistant cells, and some (e.g. *CSK*) dramatically increasing the frequency of resistant cells without a proportional change in the frequency of $NGFR^{HIGH}$ cells. One possible way to conceptualize these distinct phenotypic outcomes is that the former category of knockout affects primarily cellular variability, i.e., cellular state, while the latter affects the mapping between these states and their fates upon addition of vemurafenib. In one simple model, one could imagine a distribution of cellular states in the initial population and a threshold whereby cells above the threshold survive the drug and those below the threshold do not (Fig. 4). In this model, some knockouts may alter the distribution of cells in the initial population, thus rendering a different proportion of them above or below the threshold, or may alter the threshold itself, or potentially some combination of both. It is wise to caution against this simple interpretation, however. First, we note that NGFR expression is just a marker for the pre-resistant state, and it may be that factors may affect the frequency of pre-resistant cells without showing any effect on NGFR expression, thus giving the false appearance of a change in the mapping. (Arguing against this, however, is the fact that the transcriptomes of knockouts such as *DOT1L* that increase the frequency of NGFR and resistance appear to be similar to the profile of $NGFR^{HIGH}$ cells themselves; Fig. 3A) Further molecular profiling of individual cells from these knockouts may help reveal the ways in which the molecular state of these cells changes. Secondly, it is also likely that the categorization of fates as “resistant” or “dead” is dramatically oversimplified, and that there may be a number of different types of resistant cells (anecdotally, we have noticed that the resistant cells in some of our knockout lines do appear morphologically different from those formed in the unperturbed cell line). Such results suggest that there is a mapping from a continuum of initial cellular states to multiple, canalized, or even potentially

continuous cellular fates. An important future direction is to characterize this mapping and its regulation.

Here, we have focused on cellular variability in the context of drug resistance in cancer. However, we have observed similar rare-cell variability in primary melanocytes (*14*), raising the possibility that the same variability may play a role in normal biological processes as well. It is thus possible that the factors we have isolated may play a role in regulating variability in these normal biological contexts, and it remains to be seen whether such factors act primarily in melanocytes or act more generally across different cell types in various tissues. Indeed, we believe variability will emerge as a key aspect of cellular plasticity in general, and that framing plasticity as a mapping between variable cellular states and ultimate phenotypic fates may prove a fruitful conceptual framework.

References

1. O. Symmons, A. Raj, What's Luck Got to Do with It: Single Cells, Multiple Fates, and Biological Nondeterminism. *Mol. Cell*. **62**, 788–802 (2016).

2. A. Raj, A. van Oudenaarden, Nature, nurture, or chance: stochastic gene expression and its consequences. *Cell*. **135**, 216–226 (2008).

3. A. Raj, S. A. Rifkin, E. Andersen, A. van Oudenaarden, Variability in gene expression underlies incomplete penetrance. *Nature*. **463**, 913–918 (2010).

4. M. F. Wernet *et al.*, Stochastic spineless expression creates the retinal mosaic for colour vision. *Nature*. **440**, 174–180 (2006).

5. G. M. Süel, R. P. Kulkarni, J. Dworkin, J. Garcia-Ojalvo, M. B. Elowitz, Tunability and noise dependence in differentiation dynamics. *Science*. **315**, 1716–1719 (2007).

6. H. Maamar, A. Raj, D. Dubnau, Noise in gene expression determines cell fate in Bacillus subtilis. *Science*. **317**, 526–529 (2007).

7. M. Mojtahedi *et al.*, Cell Fate Decision as High-Dimensional Critical State Transition. *PLoS Biol.* **14**, e2000640 (2016).

8. F. Rambow *et al.*, Toward Minimal Residual Disease-Directed Therapy in Melanoma. *Cell*. **0** (2018), doi:10.1016/j.cell.2018.06.025.

9. L. A. Garraway, P. A. Jänne, Circumventing Cancer Drug Resistance in the Era of Personalized Medicine. *Cancer Discovery*. **2** (2012), pp. 214–226.

10. K. Trunzer *et al.*, Pharmacodynamic effects and mechanisms of resistance to vemurafenib in patients with metastatic melanoma. *J. Clin. Oncol.* **31**, 1767–1774 (2013).

11. S. V. Sharma *et al.*, A chromatin-mediated reversible drug-tolerant state in cancer cell subpopulations. *Cell*. **141**, 69–80 (2010).

12. P. B. Gupta *et al.*, Stochastic state transitions give rise to phenotypic equilibrium in populations of cancer cells. *Cell*. **146**, 633–644 (2011).

13. A. O. Pisco, S. Huang, Non-genetic cancer cell plasticity and therapy-induced stemness in tumour relapse: "What does not kill me strengthens me." *Br. J. Cancer*. **112**, 1725–1732 (2015).

14. S. M. Shaffer *et al.*, Rare cell variability and drug-induced reprogramming as a mode of cancer drug resistance. *Nature*. **546**, 431–435 (2017).

15. S. M. Shaffer *et al.*, Memory sequencing reveals heritable single cell gene expression programs associated with distinct cellular behaviors. *bioRxiv* (2018), p. 379016.

16. A. A. Cohen *et al.*, Dynamic proteomics of individual cancer cells in response to a drug. *Science*. **322**, 1511–1516 (2008).

17. C. Weinreb, A. E. Rodriguez-Fraticelli, F. D. Camargo, A. M. Klein, Lineage tracing on transcriptional landscapes links state to fate during differentiation. *bioRxiv* (2018), p. 467886.

18. Y. Su *et al.*, Single-cell analysis resolves the cell state transition and signaling dynamics associated with melanoma drug-induced resistance. *Proc. Natl. Acad. Sci. U. S. A.* **114**, 13679–13684 (2017).

19. M. Fallahi-Sichani *et al.*, Adaptive resistance of melanoma cells to RAF inhibition via reversible induction of a slowly dividing de-differentiated state. *Mol. Syst. Biol.* **13**, 905 (2017).

20. E. Torre *et al.*, Rare Cell Detection by Single-Cell RNA Sequencing as Guided by Single-Molecule RNA FISH. *Cell Syst* (2018), doi:10.1016/j.cels.2018.01.014.

21. I. Tirosh *et al.*, Dissecting the multicellular ecosystem of metastatic melanoma by single-cell RNA-seq. *Science*. **352**, 189–196 (2016).

22. O. Shalem *et al.*, Genome-scale CRISPR-Cas9 knockout screening in human cells. *Science*. **343**, 84–87 (2014).

23. S. Konermann *et al.*, Genome-scale transcriptional activation by an engineered CRISPR-Cas9 complex. *Nature* (2014), doi:10.1038/nature14136.

24. T. Strub *et al.*, SIRT6 haploinsufficiency induces BRAFV600E melanoma cell resistance to MAPK inhibitors via IGF signalling. *Nat. Commun.* **9**, 3440 (2018).

25. J. Joung *et al.*, Genome-scale activation screen identifies a lncRNA locus regulating a gene neighbourhood. *Nature*. **548**, 343–346 (2017).

26. C. Sun *et al.*, Reversible and adaptive resistance to BRAF(V600E) inhibition in melanoma. *Nature*. **508**, 118–122 (2014).

27. Y.-H. Huang *et al.*, POU2F3 is a master regulator of a tuft cell-like variant of small cell lung cancer. *Genes Dev.* **32**, 915–928 (2018).

28. Y. Tarumoto *et al.*, LKB1, Salt-Inducible Kinases, and MEF2C Are Linked Dependencies in Acute Myeloid Leukemia. *Mol. Cell*. **69**, 1017–1027.e6 (2018).

29. G. L. Brien *et al.*, Targeted degradation of BRD9 reverses oncogenic gene expression in synovial sarcoma. *Elife*. **7** (2018), doi:10.7554/eLife.41305.

30. F. V. Almeida, S. M. Douglass, M. E. Fane, A. T. Weeraratna, Bad company: Microenvironmentally mediated resistance to targeted therapy in melanoma. *Pigment Cell Melanoma Res.* **32**, 237–247 (2019).

31. M. L. Hartman, M. Czyz, MITF in melanoma: mechanisms behind its expression and activity. *Cell. Mol. Life Sci.* **72**, 1249–1260 (2015).

32. C. Wellbrock, I. Arozarena, Microphthalmia-associated transcription factor in melanoma development and MAP-kinase pathway targeted therapy. *Pigment Cell Melanoma Res.* **28**, 390–406 (2015).

33. B. Zhu *et al.*, The protective role of DOT1L in UV-induced melanomagenesis. *Nat. Commun.* **9**, 259 (2018).

34. M. F. Segura *et al.*, BRD4 sustains melanoma proliferation and represents a new target for epigenetic therapy. *Cancer Res.* **73**, 6264–6276 (2013).

35. M. Okada, S. Nada, Y. Yamanashi, T. Yamamoto, H. Nakagawa, CSK: a protein-tyrosine kinase involved in regulation of src family kinases. *J. Biol. Chem.* **266**, 24249–24252 (1991).

36. L. Lu *et al.*, Kdm2a/b Lysine Demethylases Regulate Canonical Wnt Signaling by Modulating the Stability of Nuclear β-Catenin. *Dev. Cell*. **33**, 660–674 (2015).

37. K. F. Harvey, X. Zhang, D. M. Thomas, The Hippo pathway and human cancer. *Nat. Rev. Cancer*. **13**, 246–257 (2013).

38. S. R. Daigle *et al.*, Selective killing of mixed lineage leukemia cells by a potent small-molecule DOT1L inhibitor. *Cancer Cell*. **20**, 53–65 (2011).

39. A. Basavapathruni *et al.*, Conformational adaptation drives potent, selective and durable inhibition of the human protein methyltransferase DOT1L. *Chem. Biol. Drug Des.* **80**, 971–980 (2012).

40. A. Subramanian *et al.*, Gene set enrichment analysis: a knowledge-based approach for interpreting genome-wide expression profiles. *Proc. Natl. Acad. Sci. U. S. A.* **102**, 15545–15550 (2005).

41. X. Bai, D. E. Fisher, K. T. Flaherty, Cell-state dynamics and therapeutic resistance in melanoma from the perspective of MITF and IFNγ pathways. *Nat. Rev. Clin. Oncol.* (2019), doi:10.1038/s41571-019-0204-6.

42. R. D. Dar, N. N. Hosmane, M. R. Arkin, R. F. Siliciano, L. S. Weinberger, Screening for noise in gene expression identifies drug synergies. *Science*. **344**, 1392–1396 (2014).

43. J. Shi *et al.*, Discovery of cancer drug targets by CRISPR-Cas9 screening of protein domains. *Nat. Biotechnol.* **33**, 661–667 (2015).

Acknowledgements
We want to thank Dr. Meenhard Herlyn for always providing excellent advice and guidance. We also thank the Flow Cytometry core, especially Florin Tuluc, at CHOP for all their advice and help. We also thank all members of the Raj Lab as well as John Murray for their comments and suggestions. We thank C. Vakoc for providing the transcription factor, epigenetic regulator, and kinase domain-focused sgRNA library. J.S acknowledges support from Linda Pechenik Montague Investigator Award and Cold Spring Harbor Laboratory sponsored research. AR acknowledges NIH/NCI PSOC award number U54 CA193417, NSF CAREER 1350601, P30 CA016520, SPORE P50 CA174523, NIH U01 CA227550, NIH 4DN U01 HL129998, NIH Center for Photogenomics (RM1 HG007743), and the Tara Miller Foundation. AW acknowledges support from CA207935 and CA174746. AW acknowledge support from CCSG P30CA010815 and NIH U01 CA227550.

Declaration of interests
A.R. and S.M.S. receives patent royalty income from LGC/Biosearch Technologies related to Stellaris RNA FISH probes. All other authors declare no competing interests.

Author contributions
E.T., J.S., and A.R. designed and supervised the study. E.T. performed the experiments and analysis. E.A., K.B. assisted with CRISPR screens. S.B. assisted with tissue culture, image acquisition, and analysis. L.B. designed image analysis software. B.E, S.S. assisted with acquisition of transcriptomic data. B.E, S.S., I.M. assisted with data analysis. A.W. provided guidance on interpretation of the data.

List of Supplementary Materials

- Materials and Methods
- Main Figures:
    - Figure 1. - Pooled CRISPR screen design to identify modulators of cellular plasticity in the context of drug resistance to targeted therapies in melanoma.
    - Figure 2. - Effects of variability hits on resistant colony formation.
    - Figure 3. - Gene set enrichment analysis of the transcriptional effects induced by the knockout of select screen targets.
    - Figure 4. - Model of adaptation thresholds and cellular heterogeneity in the development of resistance to targeted therapies.
- Supplemental Figures:
    - Supplemental Figure 1. - Effect of negative and positive control single guide RNAs in the CRISPR screens.
    - Supplemental Figure 2. - Secondary validation of hits across multiple cell lines by secondary targeted CRISPR screening.
    - Supplemental Figure 3. - Screen for factors modulating number of resistant colonies upon $BRAF^{V600E}$ inhibition (cellular “fate”).
    - Supplemental Figure 4. - Secondary validation of hits across multiple cell lines by secondary targeted CRISPR screening
    - Supplemental Figure 5. - Validation of effects on state and fate of variability hits by via NGFR immunofluorescence and resistant colony formation.
    - Supplemental Figure 6. - Validation of effects on fate of variability hits by resistant colony formation.
    - Supplemental Figure 7. - Effect of pharmacological inhibition of DOT1L on resistance to $BRAF^{V600E}$ and MEK inhibition.
    - Supplemental Figure 8. - Percent of targets from the state screen that validate.
    - Supplemental Figure 9. - Percent of targets from the fate screen that validate.
    - Supplemental Figure 10. - Transcriptional effects induced by knockout of select screen targets.
    - Supplemental Figure 11. - Technical validation of WM989-A6-G3-Cas9-5a3 cell line.
- Supplemental Tables:
    - Supplemental Table 1. - sgRNA sequences of initial screens - Epigenetic targets
    - Supplemental Table 2. - sgRNA sequences of initial screens - Kinase targets
    - Supplemental Table 3. - sgRNA sequences of initial screens - Transcription factor targets
    - Supplemental Table 4. - Master table with results from genetic screens and their follow up experiments
    - Supplemental Table 5. - Targets included secondary screen
    - Supplemental Table 6. - Groups of gene sets

Supplemental Materials

Material and Methods

Cell Culture

We obtained patient-derived melanoma cells (WM989 and 451Lu, female and male, respectively) from the lab of Meenhard Herlyn. For WM989 we derived a single cell subclone (A6-G3) in our lab (*14*). We grew these cells at 37°C in Tu2% media (78% MCDB, 20% Leibovitz's L-15 media, 2% FBS, and 1.68mM CaCl2). We authenticated all cell lines via Human STR profiling. We periodically tested all cell lines for mycoplasma infections.

Plasmid Construction and single guide RNA Cloning

All the Cas9 positive melanoma cell lines in this study were derived by lentiviral transduction with a Cas9 expression vector (EFS-Cas9-P2A-Puro, Addgene: 108100). All the single guide RNAs were cloned into a lentiviral expression vector LRG2.1(Addgene: #108098), which contains an optimized single guide RNA backbone. The annealed single guide RNA oligos were T4 ligated to the BsmB1-digested LRG2.1 vector. To improve U6 promoter transcription efficiency, an additional 5' G nucleotide was added to all single guide RNA oligo designs that did not already start with a 5' G.

Construction of Domain-Focused single guide RNA Pooled Library

Gene lists of transcription factors (TF), kinases, and epigenetic regulators in the human genome were manually curated based on the presence of DNA binding domain(s), kinase domains, and epigenetic enzymatic/reader domains. The protein domain sequence information was retrieved from NCBI Conserved Domains Database. Approximately 6 independent single guide RNAs were designed against individual DNA binding domains (Supplementary tables 1-3).(*27–29*) The design principle of single guide RNA was based on previous reports and the single guide RNAs with the predicted high off-target effect were excluded (Hsu et al., 2013). For the initial pooled CRISPR screen, all of the single guide RNAs oligos including positive and negative control single guide RNAs were synthesized in a pooled format (Twist Bioscience) and then amplified by PCR. PCR amplified products were cloned into BsmB1-digested LRG2.1 vector using Gibson Assembly kit (NEB#E2611). For the targeted pooled validation screen, individual single guide RNAs were synthesized, cloned, and verified via Sanger sequencing in a 96-well array platform (Supplementary table 5). Individual single guide RNAs were pooled together in an equal molar ratio. To verify the identity and relative representation of single guide RNAs in the pooled plasmids, a deep-sequencing analysis was performed on a MiSeq instrument (Illumina) and confirmed that 100% of the designed single guide RNAs were cloned in the LRG2.1 vector and the abundance of >95% of individual single guide RNA constructs was within 5-fold of the mean (data not shown).

Lentivirus preparation
We produced lentivirus containing single guide RNAs using HEK293T cells cultured in DMEM supplemented with 10% Fetal Bovine Serum and 1% penicillin/streptomycin. When the cells reached 90-100% confluency, we mixed the single guide RNA vectors with the packaging vector psPAX2 and envelope vector pVSV-G in a 4:3:2 ratio in OPTI-MEM (ThermoFisher Scientific: #31985070) and polyethylenimine (PEI, Polysciences: #23966). We collected viral supernatants for up to 72 hours twice daily.

Transduction of spCas9
We introduced the stable expression of spCas9 via spinfection of lentivirus along with 5ug/ml polybrene for 25 minutes at 1750 rpm. We exchanged the media ~6 hours post-transduction and selected for cells expressing spCas9 via puromycin selection (1-2µg/ml, 1 week). For WM989-A6-G3, we generated two cell lines, WM989-A6-G3-Cas9 and WM989-A6-G3-Cas9-5a3, the later being a single cell isolate of the bulk Cas9-expressing population. We verified that this cell line was capable of editing the genome and that it still contained pre-resistant cells marked by the expression of drug-resistance markers (Supplemental Fig. 11).Following the same methodology, we generated a 451Lu-Cas9 cell line from 451Lu cells.

Transduction of lentivirus containing single guide RNAs
For transfection of melanoma cells, we infected cells with lentivirus and 5ug/ml polybrene for 25 minutes at 1750 rpm. We exchanged the media ~6 hours post-transfection. We quantified the percent of the population transfected by measuring the number of GFP-positive cells at day 5 post-transfection. For the screens, we aimed to transfect 30% of the population. For all other experiments, we aimed to transfect >95% of the population.

Initial pooled CRISPR screens
We worked with three main pooled single guide RNA libraries in WM989-A6-G3-Cas9-5a3 cells. These libraries targeted ~2,000 different kinases, transcription factors, and proteins involved in epigenetic regulation. In total, the libraries contained ~13,000 different single guide RNAs including non-targeting and cell-viability editing controls (Supplementary tables 1-3). We aimed to transfect > 1,000 cells per single guide RNA and isolated ~1,000 cells per single guide RNA about a week post-transfection and prior to any selection. These baselines allowed us to validate the efficiency of our screen by single guide RNA enrichment/depletion of non-targeting controls and of controls that affect cell viability (Supplemental Fig. 1). Additionally, these baselines helped us identify single guide RNAs with lethal effects in our cells. Given that we were interested in rare cell phenotypes that exist in 1:2000 cells or less, throughout our screens we significantly expanded the population of cells to 50,000-250,000 cells per single guide RNA, often surpassing a billion cells per screen. This scale allowed us to observe the rare cell phenotypes dozens-to-hundreds of times in each of our controls (and in each of our single guide RNAs).

The state screen aimed to identify perturbations that altered the frequency of $NGFR^{HIGH}/EGFR^{HIGH}$ cells. To this end, one month after we transfected and expanded the cells, we isolated the $NGFR^{HIGH}/EGFR^{HIGH}$ cells via magnetic cell sorting (MACS) followed by fluorescence-activated cell sorting (FACS) (see below). We also collected an additional ~1,000 cells per single guide RNA, without any selection, for comparison. Then, we isolated DNA from the cells and built sequencing libraries (see below) to quantify the representation of each single guide RNA in the $NGFR^{HIGH}/EGFR^{HIGH}$ population and compare it to the unsorted baseline.

In the fate screen we aimed to identify proteins important for the development of resistance to vemurafenib. Here, we treated the cells as above, except that instead of isolating $NGFR^{HIGH}/EGFR^{HIGH}$ cells we grew cells resistant to vemurafenib (see below) by exposing the cells to vemurafenib for three weeks. As above, we isolated DNA from the resulting population of cells and built sequencing libraries to quantify the representation of each single guide RNA. The raw output of all screens was reads per single guide RNA.

To select hits in our screens, we first normalized the output of our screens to reads per million, and then calculated the fold change in single guide RNA representation between different samples. For our state screen, we focused on the fold change in single guide RNA representation between $NGFR^{HIGH}/EGFR^{HIGH}$ cells and the bulk population of melanoma cells. For the fate screen, we focused on the fold change in single guide RNA representation between cells treated for three weeks with 1μM vemurafenib (a $BRAF^{V600E}$ inhibitor) and cells never exposed to the drug. After normalizing the change in single guide RNA representation of each single guide RNA by the median change across all single guide RNAs, we organized our hits into tiers (one through four) based on the percent of single guide RNAs against the target exhibiting at least a two-fold change in representation. We considered high confidence hits those targets where (1) ≥ 66% of its single guide RNAs showed at least a two-fold enrichment/depletion throughout the screen, and (2) no two single guide RNAs showed a significant change (two-fold change) in opposing directions (i.e. one single guide RNA is significantly enriched in the selected population while another one is significantly depleted). Other targets that showed a two-fold enrichment/depletion throughout the screen, but in less than 66% of its single guide RNAs were considered lower confidence hits. Note that we excluded from analysis any single guide RNA with less than 10 raw reads in all samples.

Secondary, targeted pooled CRISPR screen

To validate the replicability and generality of our hits, we designed a pool of single guide RNAs for targeted screening that targeted proteins that either emerged as hits in our initial screens or did not pass our hit-selection criteria but changed the frequency of $NGFR^{HIGH}/EGFR^{HIGH}$ cells or the frequency of cells resistant to vemurafenib (Supplemental Table 5). In this pool, we included ~3 single guide RNAs per protein target, and carried out the screen in WM989-A6-G3-Cas9-5a3 cells as well as in another $BRAF^{V600E}$ melanoma cell line, 451Lu-Cas9. As before, we conducted a state screen where we isolated $NGFR^{HIGH}/EGFR^{HIGH}$ cells as well as a fate screen where we exposed cells to 1μM vemurafenib for three weeks. Here too, we first normalized the output of our screens to reads per million, and then calculated the fold change in single guide RNA

representation between different samples. Unlike on our initial screens, here we normalized the change in single guide RNA representation to the median change in representation of the ten non-targeting single guide RNAs controls included in the screen.

Immunostains

For NGFR stain of fixed cells, after fixation and permeabilization, we washed the cells for 10 min with 0.1% BSA-PBS, and then stained the cells for 10 min with 1:500 anti-NGFR APC-labelled clone ME20.4 (Biolegend, 345107). After two final washes with PBS we kept the cells in PBS. For EGFR and NGFR stains of live cells, we incubated melanoma cells in suspension for 1 hour at 4C with 1:200 mouse anti-EGFR antibody, clone 225 (Millipore, MABF120) in 0.1% BSA PBS. We then washed twice with 0.1% PBS-BSA and then incubated for 30 minutes at 4C with 1:500 donkey anti-mouse IgG-Alexa Cy3 (Jackson Laboratories, 715-545-150). We washed the cells again (twice) with 0.1% BSA-PBA and incubated for 10 minutes with 1:500 anti-NGFR APC-labelled clone ME20.4 (Biolegend, 345107). We again washed the cells twice with 0.1% BSA-PBS and finally re-suspended them in 1%BSA-PBS.

Isolation of pre-resistant cells (MACS + FACS)

To enrich for $NGFR^{HIGH}$/$EGFR^{HIGH}$ cells we first immunostained melanoma cells as detailed above. Then, we used a Manual Separator for Magnetic Cell Isolation (MACS, with LS columns and Anti-APC microbeads). In short, following the manufacturer's instructions, we incubated cells and microbeads at 4C for 15 min, then washed and pelleted the cells via centrifugation. After resuspending the cells, we passed them through LS magnetic columns. After enriching for $NGFR^{HIGH}$ cells, we proceeded to select only the cells expressing both NGFR and EGFR via Fluorescent-Activated Cell Sorting (FACS, MoFlo Astrios EQ).

Growth of resistant colonies

To grow melanoma cells resistant to $BRAF^{V600E}$ inhibition, we exposed melanoma cells to 1μM vemurafenib (PLX4032, Selleckchem S1267) for 2-3 weeks. For the $BRAF^{V600E}$ and MEK co-inhibition assays, we also used dabrafenib at 500nM and 100nM (GSK2118436, Selleckchem S2807), trametinib at 5nM and 1nM (GSK1120212, Selleckchem S2673), and cobimetinib at 10nM and 1nM (GDC-0973, Selleckchem S8041).

Inhibition of DOT1L via small molecule inhibitor

For all assays involving pharmacological inhibition of DOT1L we used pinometostat at concentrations ranging from 1μM to 5μM (EPZ5676, Selleckchem S.7062).

MiSeq library construction and sequencing

In order to quantify the single guide RNA representation following selection in our screen we sequenced the single guide RNAs as per (*43*). In short, we isolated genomic DNA using the Quick-DNA Midiprep Plus Kit (Zymo Research: #D4075) per manufacturer specifications. We then PCR-amplified the single guide RNAs using Phusion Flash High Fidelity Master Mix Polymerase (Thermo Scientific: #F-548L) and primers that incorporate a barcode and a sequencing adaptor to the amplicon. Our amplification strategy consisted of an initial round of

parallel PCRs (23-29 cycles of up to 200 parallel reactions per sample. We then pooled the PCR reactions and purified them using the NucleoSpin® Gel and PCR Clean-up kit (Macherey-Nagel: #740609.250). We continued with eight PCR cycles using Phusion Flash High Fidelity Master Mix Polymerase, followed by column purification with the QIAquick PCR Purification Kit (QIAGEN: #28106). We quantified the single guide RNA libraries with the DNA 1000 Kit (Agilent: #5067-1504) on a 2100 Bioanalyzer Instrument (Agilent: #G2939BA). We pooled the barcoded single guide RNA libraries and sequenced via 150-cycle paired-end sequencing (MiSeq Reagent Kit v3, Illumina: #MS-102-3001). We then mapped the resulting sequences to our reference single guide RNA library and proceeded to select hits.

Cell fixation and permeabilization

For our imaging assays we fixed cells for 10 min with 4% formaldehyde and permeabilized them with 70% ethanol overnight.

Colony formation assays

For each condition tested, we first plated cells in duplicate (~10-50,000 cells per well of a 6-well plate). We fixed and permeabilized one of the duplicates to use as a baseline and exposed the second duplicate to the test condition. At the endpoint, we fixed and permeabilized the second duplicate.

Image analysis of NGFR immunostains

We developed a custom MATLAB pipeline for counting cells and quantifying immunofluorescence signal of DAPI-stained and NGFR-stained cells (https://bitbucket.org/arjunrajlaboratory/rajlabscreentools/src/default/). The software stitches together a large tiled image, then uses DAPI to identify cells. Using the nuclear area, it then looks at a set of pixels near the nucleus to quantify fluorescence intensity of the NGFR staining. After quantifying the expression level of NGFR following knockout of select screen targets and of non-targeting controls, we quantified the minimum expression level needed to be considered an $NGFR^{HIGH}$ cell. First, we selected the top one percent highest expressors of NGFR in each of our non-targeting negative controls. Then, within that top one percent we obtained the median expression level of the lowest expressor across all controls, and used that as a threshold to quantify the frequency of $NGFR^{HIGH}$ cells in each of our knockout samples. Then, we calculated the change in frequency of $NGFR^{HIGH}$ cells in each test condition compared to controls and obtained a median fold change and standard deviation across all samples with knockout of one same protein (~3 different biological samples per protein). In total, we targeted ~86 different proteins across ~258 different knockout biological samples.

Image analysis of colony formation

We developed a custom MATLAB pipeline for counting cells and colonies in tiled images of DAPI-stained cells (https://bitbucket.org/arjunrajlaboratory/colonycounting_v2/src/default/). First, the software stitches the individual image tiles into one large image by automatically (or with user input) determining the amount of overlap between each individual image. Then, the software identifies the location of each cell in the stitched image by searching for local maxima.

We then manually identify the colony boundaries and quantify the number of colonies in each sample. We then calculate the frequency of resistant colonies by dividing the number of colonies by the total number of cells present in culture prior to $BRAF^{V600E}$ inhibition. Finally, we scale the frequency of colonies to colonies per 10,000 cells and calculate the change in frequency between each sample and the median change across controls.

RNA-sequencing and identification of differential expression

We sequenced mRNA in bulk from WM989-A6-G3 and WM989-A6-G3-Cas9 populations as per Shaffer et. al. In addition to quantifying the transcriptome of $EGFR^{HIGH}$cells, $NGFR^{HIGH}$, $NGFR^{HIGH}$/$EGFR^{HIGH}$ cells and vemurafenib-resistant cells, we quantified the transcriptional changes following the knockout of many tier 1 and tier 2 hits from both the state and fate screens. In addition to hits from our screens, we also quantified the transcriptome of targets that were not tier 1 or tier 2 hits, but show a change in the frequency of $NGFR^{HIGH}$/$EGFR^{HIGH}$ cells or of cells resistant to vemurafenib. In total, we targeted ~83 different proteins, each in triplicate (using different single guide RNAs) for a total of 280+ RNA sequencing samples. For each sample, we isolated mRNA and built sequencing libraries using the NEBNext Poly(A) mRNA Magnetic Isolation Module and NEBNext Ultra RNA Library Prep Kit for Illumina per manufacturer instructions. We then sequenced the libraries via paired-end sequencing (36x2 cycles) on a NextSeq 500. We aligned reads to hg19 and quantified reads per gene using STAR and HTSeq. We then used DEseq2 to identify differentially expressed genes.

Gene set enrichment analysis

To identify “biological signatures” enriched or depleted following the knockout of a given target we used the GSEA software (http://software.broadinstitute.org/gsea/index.jsp). We focused in the Biological Process ontology of the Gene Ontology gene sets (http://geneontology.org) to obtain enrichment scores.

Grouping of targets based on transcriptomic analysis

To group targets into classes based on their transcriptional effects, we clustered all RNA-seq samples (hierarchical clustering via pheatmap in R) based on the change in expression (as obtained by DEseq2) of any gene differentially expressed (two-fold change over control, with an adjusted p value ≤ 0.05) in at least one of the 83+ knockouts. We also grouped targets via pheatmap based on the enrichment scores obtained via GSEA. To identify the axes that account for the variability between each knockout we also performed principal component analysis based on the gene set enrichment scores of each knockout. Note that in the aforementioned analysis we included the transcriptomes of pre-resistant cells (marked by the expression of EGFR alone, NGFR alone, and NGFR and EGFR in combination) and of cells resistant to vemurafenib.

Software and data availability

All data and code used for the analysis can be found at
https://www.dropbox.com/sh/t08558cl4mepfm6/AABBvbtlTPSNNPoMC9NTro-9a?dl=0

The software used for colony growth image analysis can be found at: https://bitbucket.org/arjunrajlaboratory/colonycounting_v2/src/default/ . The software used for analysis of immunofluorescence images can be found at: https://bitbucket.org/arjunrajlaboratory/rajlabscreentools/src/default/

Main Figure legends

Figure 1. Pooled CRISPR screen design to identify modulators of cellular plasticity in the context of drug resistance to targeted therapies in melanoma.

A. (top) In melanoma, the initial molecular profile (i.e., "state") of a cell within an otherwise homogeneous population, indicated by green vs. gray coloring of cell, dictates the ultimate fate of the cell (e.g. proliferation vs. death). Changing the number of cells in a given state (A, middle) or the mapping between state and fate (A, bottom) can alter the number of resistant colonies that form upon addition of the $BRAF^{V600E}$ inhibitor vemurafenib.

B. We designed a pooled CRISPR screen to detect modulators of the rare cellular states that lead to drug resistance. After transducing a library of single guide RNAs and expanding the population, we isolated cells with high expression of both NGFR and EGFR, then sequenced the single guide RNAs to determine which gene knockouts alter the frequency of these cells. Changes in the frequency of a given single guide RNA in this population (e.g. targets A and C) indicate that these targets may affect the frequency of $NGFR^{HIGH}/EGFR^{HIGH}$ cells in the population, and thus may affect the cellular state associated with pre-resistance.

C. After transducing a population of melanoma cells and isolating $NGFR^{HIGH}/EGFR^{HIGH}$ cells (see Fig. 1B), we quantified the frequency of each single guide RNA in the resulting population. Our screening scheme utilized three separate pooled single guide RNA libraries, one targeting epigenetic domains (top left), another targeting kinases (bottom left), and a final one targeting transcription factors (right). We organized the targets within each single guide RNA library by biological process. (While a given target could fall into several categories, each target is assigned to a single group and plotted only once.) Each dot represents a single guide RNA, grouped by gene target (5-6 single guide RNAs per target), with the $\log_2$ fold change representing the number of times the single guide RNA was detected in the sorted population versus an unsorted population of melanoma cells transduced with the same library. For display purposes, all single guide RNAs with fold changes beyond the axis limits were placed at the edge of the axis as indicated. For targets considered "hits" by our rubric (see methods), we labeled the single guide RNA dot by the color assigned to that biological process. Dots at the bottom of each pane correspond to non-targeting controls (single guide RNAs not targeting any loci in the genome) and cell viability controls (e.g. proteins required for cell survival and proliferation, but not specifically associated with rare-cell behavior). Supplemental Fig. 1 provides details on the effect of these editing controls.

D. Effect overlap between state and fate hits. Each target's position (dots) represents the number of times (as median log2 fold change) the single guide RNAs were detected in the $NGFR^{HIGH}/EGFR^{HIGH}$ population vs. an unsorted population of melanoma cells (state screen, x-axis), or in the population of cells resistant to vemurafenib vs. the population of cells prior to

treatment (fate screen, y-axis). Orange labels correspond to high confidence targets (Tier 1 and Tier 2) in the state screen; blue corresponds to high confidence targets in the fate screen; purple corresponds to high confidence targets in both screens. The effects of all targets in both screens are displayed as a density histogram.

Figure 2. Effects of variability hits on resistant colony formation.
A. To validate the phenotypic effect of targets identified by our genetic screen, we knocked out 83 of the targets and quantified both the frequency of $NGFR^{HIGH}$ cells by immunofluorescence using anti-NGFR antibodies (top) and the number of resistant colonies (bottom) that form upon $BRAF^{V600E}$ inhibition. Here we show example state and fate validation of BRD2 and LATS2 knockouts. The schematic represents the effect of the knockout in the state screen on the frequency of $NGFR^{HIGH}$/$EGFR^{HIGH}$ cells.
B. Relationship between the frequency of $NGFR^{HIGH}$ cells (x-axis) and the number of resistant colonies (y-axis). We plot the frequency of $NGFR^{HIGH}$ cells as the mean $\log_2$ fold change over three replicates in the number of $NGFR^{HIGH}$ cells following knockout of the gene indicated, normalized by cells with non-targeting sgRNAs. (For variability of the effect size across replicates of a given target, see Supplemental Fig. 5). We quantified the $\log_2$ fold change in the number of resistant colonies in the knockout cell line as compared to the non-targeting control cell lines. Orange points are targets identified as high confidence hits (Tier 1 and Tier 2) in the state screen; blue are those identified as high confidence hits in the fate screen; purple are those identified as high confidence hits in both state and fate screen; gray, those that may have shown an effect in either or both screens, but were not classified as high confidence hits in either screen.
C. To assess the effect of DOT1L inhibition (green arrows, pinometostat at 4μM) at different times on a cell's ability to survive $BRAF^{V600E}$ inhibition, we first established a baseline number of colonies that grow when WM989-A6-G3 cells are exposed to 1μM of vemurafenib for three weeks (leftmost panel). Then, in a separate population, we either inhibited $BRAF^{V600E}$ and DOT1L simultaneously (co-treatment), inhibited DOT1L first (seven days) and then $BRAF^{V600E}$ (three additional weeks; pre-treatment), or inhibited DOT1L before (seven days) and during three weeks of vemurafenib treatment (pre-treatment and co-treatment).
D. Number of resistant colonies that result from each therapeutic regimen in Fig. 2C as the mean fold change over baseline (vemurafenib alone) for three replicates normalized to the number of cells in culture prior to $BRAF^{V600E}$ inhibition. Error bars indicate the standard error of the mean over triplicates.

Figure 3. Gene set enrichment analysis of the transcriptional effects induced by the knockout of select screen targets.
A. The heatmap represents biclustering analysis of different knockout cell lines (rows) based on the Gene Set Enrichment Analysis score of Gene Ontology gene sets (Biological process GO terms, columns in heatmap). Within the heatmap, red indicates enrichment in the sense that there are more differentially upregulated genes in knockout vs. control in that gene set than expected by chance, whereas blue indicates enrichment of downregulated genes (shade indicates degree of enrichment). Each target knockout (rows) represents transcriptomes of

biological triplicates (unless otherwise stated on Supplemental Table 4). Target labels (rows) in green indicate genes whose knockout increased the frequency of $NGFR^{HIGH}/EGFR^{HIGH}$ cells in the screen, while red indicates targets whose knockout increased the number of cells resistant to vemurafenib, and gray indicates targets that decreased the frequency of either $NGFR^{HIGH}/EGFR^{HIGH}$ cells or of cells resistant to vemurafenib. As before, we organized targets into high confidence hits (Tier 1 and Tier 2) and low confidence hits (Tiers 3 and Tier 4) based on the percentage of single guide RNAs against a target that showed at least a two-fold change in the initial screen (see knockout color key).The asterisks next to the label indicate the tier (Tier 1, ****; Tier 2, ***; Tier 3, **; Tier 4, *). Based on the dendrogram on the left, we grouped targets into six clusters. We also clustered gene sets (columns) into groups, labeled by the letters on top of the heatmap. The white boxes inside the heatmap demark groups of gene sets specifically upregulated in a given cluster.
B. Select list of gene sets in groups D and E from Figure 3A. For a complete list of gene sets within each group, see supplementary table 6.
C. Relationship between the expression of genes involved in neural crest differentiation (x-axis) and the number of colonies resistant to vemurafenib (y-axis) following the knockout of a target. For each knockout, we plot the expression of neural crest differentiation genes as the enrichment score obtained through gene set enrichment analysis for the neural crest differentiation gene set (GO term). We quantified the $\log_2$(fold change) in the number of resistant colonies in the knockout cell line as compared to the non-targeting control cell lines. Colors represent the cluster grouping of each knockout based on Figure 3A.
D. Relationship between the frequency of $NGFR^{HIGH}$ cells (x-axis) and the number of resistant colonies (y-axis). As in Fig. 2B, we plot the frequency of $NGFR^{HIGH}$ cells as the median $\log_2$(fold change) over three replicates in the number of $NGFR^{HIGH}$ cells following knockout of the indicated gene normalized by cells with non-targeting single guide RNAs. (For variability of the effect size across replicates of a given target, see Supplemental Fig. 5.) We quantified the $\log_2$(fold change) in the number of resistant colonies in the knockout cell line as compared to the non-targeting control cell lines. We color-coded all targets by groupings based on their transcriptomes (see Fig. 3A) following knockout of the gene indicated.

Figure 4. Model of adaptation thresholds and cellular heterogeneity in the development of resistance to targeted therapies. Variability in the expression of various markers are associated with an individual cell's probability to survive drug treatment. In one simple model, cellular variability occurs along a single ordinate, which can be conceptualized as the degree of "greenness". Operationally, this may be related to the expression of a marker of pre-resistance, such as *NGFR*. In this model, there is a threshold (red line, top panel) that divides cells along this axis into those that adapt to the drug and become resistant vs. those that no longer proliferate when challenged with drug. Here, there are at least two ways by which one could conceivably alter the number of cells that survive the drug. In one scenario (middle) the distribution of "greenness" could change, leading to more cells being above the threshold, leading to more resistant colonies. In another scenario, the distribution of phenotypes remains unchanged, but the threshold itself moves, also leading to more resistant colonies. Our results

suggest (but do not prove) that both scenarios may play out to varying degrees as a result of different genes being knocked out.

Supplemental Figure legends

Supplemental Figure 1. Effect of negative and positive control single guide RNAs in the CRISPR screens. Our pooled CRISPR screen included non-targeting single guide RNAs as negative controls (gray bars, 50+ single guide RNAs) as well as single guide RNAs affecting cell viability as positive controls (red bars, 25+ single guide RNAs). We quantified the change in representation of these single guide RNAs over time and report the $\log_2$ fold change in representation from six days after transfection to right before selection (vemurafenib exposure or selection by NGFR and EGFR expression). We expect positive controls to lose representation over time more often than negative controls. Our screening scheme utilized three separate pooled single guide RNA libraries, one targeting kinases (top), another targeting epigenetic domains (middle), and a final one targeting transcription factors (bottom).

Supplemental Figure 2. Secondary validation of hits across multiple cell lines by secondary targeted CRISPR screening.
We assessed the robustness and generality of the effect of hits identified in the state screen (WM989-A6-G3-Cas9-5a3, black bars) by carrying out a secondary screen containing single guide RNAs for 34 of the high confidence hits (Tiers 1 and 2) we identified in the state screen, as well as another 52 lower confidence factors from Tiers 3 and 4 (these lower confidence hits may also have been high confidence hits in the “fate” screen). See Supplemental Table 5 for a list of the targets. We carried out this screen in WM989-A6-G3-Cas9 (orange bars) as well as in another $BRAF^{V600E}$ melanoma cell line (451Lu-Cas9, blue). Within each tier, names labeled in green correspond to targets whose single guide RNAs are enriched in $NGFR^{HIGH}/EGFR^{HIGH}$ cells in the initial screen and gray represents targets whose single guide RNAs are underrepresented in these rare cells. We plotted the median $\log_2$ fold change in single guide RNA representation (normalized by non-targeting controls) across three single guide RNAs. Error bars represent the standard deviation of the fold change across all single guide RNAs for a given target. Dotted error bars in red extend beyond the limits of the graph. Note that the limits of the axes vary between tiers. We found that 25 of the 34 high confidence hits showed at least a two fold change in the frequency of $NGFR^{HIGH}/EGFR^{HIGH}$ cells concordant with the effects detected in the original screening clonal cell line (WM989-A6-G3-Cas9-5a3). In 451Lu-Cas9 cells, 20 of the 34 targets also showed a change in the frequency of $NGFR^{HIGH}/EGFR^{HIGH}$ cells, with 11 of those exhibiting at least a two-fold change. Although quantitatively they were not as strong as the effects of the Tier 1 and 2 hits, even Tier 3 and 4 hits displayed qualitative agreement in these secondary screens.

Supplemental Figure 3. Screen for factors modulating number of resistant colonies upon $BRAF^{V600E}$ inhibition (cellular “fate”).

A. We performed a pooled CRISPR screen to detect modulators of cellular fate (e.g. number of drug-resistant colonies) in the presence of the $BRAF^{V600E}$ inhibitor vemurafenib. After transducing a library of single guide RNAs and expanding the population, we exposed the cells to the $BRAF^{V600E}$ inhibitor vemurafenib (1μM) for 3 weeks, after which we sequenced the single guide RNAs in the surviving population. Changes in the frequency of detection of a given single guide RNA indicates that its target may affect the ability of a cell to survive and proliferate upon $BRAF^{V600E}$ inhibition.
B. After transfecting a population of melanoma cells, we exposed them to vemurafenib ($BRAF^{V600E}$ inhibitor, 1μM) for three weeks to grow resistant colonies. We then sequenced the DNA to quantify the single guide RNA representation of each target in the resulting population, using the same libraries as in Fig. 2. As before, we ranked the targets into tiers based on the percent of single guide RNAs that exhibited at least a two-fold change in representation throughout the screen (Tier 1, ≥ 75%; Tier 2, ≥ 66%; Tier 3, ≥ 50%; Tier 4, < 50%), thus reflecting the degree of confidence we have in the hit (High confidence hits: Tiers 1 and 2; Low confidence hits: Tiers 3 and 4). In this screen, we identified 24 high confidence factors. For a more detailed description see the methods section.

Supplemental Figure 4. Secondary validation of hits across multiple cell lines by secondary targeted CRISPR screening.
We assessed the robustness and generality of the effect of hits identified in the initial fate screen (WM989-A6-G3-Cas9-5a3, black bars) by carrying out a secondary screen containing single guide RNAs for nine high confidence targets (as well as 77 targets that either affected vemurafenib resistance but did not pass the thresholds to be called a hit, or affected the frequency of $NGFR^{HIGH}$/$EGFR^{HIGH}$ cells; Supplemental Table 5 for a list of all the targets). We carried out this screen in WM989-A6-G3-Cas9 (orange bars) as well as in another $BRAF^{V600E}$ melanoma cell line (451Lu-Cas9, blue). Within each tier, names labeled in red correspond to targets whose single guide RNAs are enriched in cells resistant to vemurafenib in the initial screen and gray represents targets whose single guide RNAs are underrepresented in these cells. We plotted the median $\log_2$ fold change in single guide RNA representation (normalized by non-targeting controls) across three single guide RNAs. Error bars represent the standard deviation of the fold change across all single guide RNAs for a given target. Dotted error bars in red extend beyond the limits of the graph. Note that the limits of the axes vary between tiers. In WM989-A6-G3-Cas9, we found that seven of the nine targets replicated the effect that we observed originally. For 451Lu-Cas9, the same seven factors showed similar effects.

Supplemental Figure 5. Validation of effects on state and fate of variability hits by via NGFR immunofluorescence and resistant colony formation.
A. Frequency of $NGFR^{HIGH}$ cells following the knockout of select targets. Each bar represents the change in the number of $NGFR^{HIGH}$ cells following knockout of the gene indicated over replicates, each using a different single guide RNA. Error bars represent the standard error of the mean across the replicates. We carried out each measurement over three replicates, but excluded samples with low cell density (< 500 cells). The star above or below the bars indicate targets where, after excluding samples with low cell numbers, n = 1. Tier refers to the degree of

confidence we have in each particular hit, with tier 1 representing highest confidence hits for which ≥ 75% of the single guide RNAs passed a threshold of two-fold change in the initial state screen. We performed this analysis for hits from both the state screen (top) and the fate screen (bottom). 21 of 34 high confidence hits from the state screen showed at least a 50% increase or decrease in the frequency of $NGFR^{HIGH}$ cells over control. Of the lower confidence hits (Tier 3 and Tier 4) 21 out of 49 targets increased or decreased the frequency of $NGFR^{HIGH}$ cells by 50% or more.

B. Resistance phenotype of melanoma cells following the knockout of hits from the initital screens. Each bar represents the $\log_2$ fold change over non-targeting control in the number colonies able to grow in vemurafenib following knockout of the gene indicated. The number of colonies for each target is normalized to the number of cells present in culture before $BRAF^{V600E}$ inhibition, reported as number of colonies per every 10,000 cells in culture prior to treatment (see methods). As before, the different tiers represent the percent of single guide RNAs against a given target exhibiting at least a two-fold change throughout the initial (left) state or (right) fate screens. On the left panel, we labeled in green and gray the effect a given target has in the frequency of $NGFR^{HIGH}$/$EGFR^{HIGH}$ cells (based on the initial state screen). On the right panel, we labeled in red and gray the effect a given target has in the number of cells that resist $BRAF^{V600E}$ inhibition (based on the initial fate screen). In this plot each bar represents one experimental replicate. See Supplemental Fig. 6 for replicates.

C. These images show the effect of CSK knockout on a cell's ability to develop resistance to $BRAF^{V600E}$ inhibition. Here, we plated CSK-knockout WM989-A6-G3-Cas9-5a3 cells and exposed them to 1μM vemurafenib for three weeks. As before, after the treatment we counted the number of resulting colonies and compared it to the number of colonies resulting from WM989-A6-G3-Cas9-5a3 cells without the knockout. Note that the number of resistant cells in the CSK sample is too large to accurately identify individual colonies. We only counted colonies we could clearly delineate, and thus, the number of colonies reported is an underestimate.

Supplemental Figure 6. Validation of effects on fate of variability hits by resistant colony formation. Resistance phenotype of melanoma cells following the knockout of hits from the initial screens. Each bar represents the $\log_2$ fold change over non-targeting control in the number of colonies able to grow following knockout of the gene indicated. The number of colonies for each target is normalized to the number of cells present in culture before $BRAF^{V600E}$ inhibition, reported as number of colonies per every 10,000 pre-treatment cells (see methods). As before, the different tiers represent the percent of single guide RNAs against a given target exhibiting at least a two-fold change throughout the initial (top) state or (bottom) fate screens. On the top panel, we labeled in green and gray the effect a given target has in the frequency of $NGFR^{HIGH}$/$EGFR^{HIGH}$ cells (based on the initial state screen). On the bottom panel, we labeled in red and gray the effect a given target has in the number of cells that resist $BRAF^{V600E}$ inhibition (based on the fate screen). In this plot each bar represents one experimental replicate (distinct from the one in Supplemental Fig. 5B).

Supplemental Figure 7. Effect of pharmacological inhibition of DOT1L on resistance to $BRAF^{V600E}$ and MEK inhibition.

A. Resistance phenotype of melanoma cells following pharmacological inhibition of DOT1L. We pre-treated melanoma cells for seven days with either DMSO, or various concentrations of the DOT1L inhibitor pinometostat (EPZ5676). Then, we exposed the cells to 1μM vemurafenib for three weeks.
B. To assess the effect of DOT1L inhibition on cellular proliferation, we the compared the population size of WM989-A6-G3 cells over time treated with either 4μM of pinometostat (DOT1L inhibitor) or with DMSO. The population size is estimated by the amount of nucleic acids present in the population using a CyQuant GR dye. The values represent mean fluorescence signal over triplicates. Error bars represent standard error of the mean.
C. Resistance phenotype of melanoma cells to $BRAF^{V600E}$ and MEK inhibitors following pharmacological inhibition of DOT1L. We pre-treated melanoma cells for seven days with either DMSO or 4μM of pinometostat. We then exposed the cells to one of two $BRAF^{V600E}$ inhibitors (vemurafenib and dabrafenib, left panels), to one of two MEK inhibitors (cobimetinib and trametinib, middle panels), or to a combination of a $BRAF^{V600E}$ and MEK inhibitor (vemurafenib + cobimetinib; dabrafenib + trametinib, right panels). White arrows point to a few of the many colonies that grew under each condition.

Supplemental Figure 8. Percent of targets from the state screen that validate. To assess the sensitivity of our screen, we validated the effect observed in the initial state screen for a select group of targets via NGFR immunofluorescence. Here, each dot represents an individual single guide RNA, and we plot the change in single guide RNA representation between $NGFR^{HIGH}$/$EGFR^{HIGH}$ cells and controls (as measured in the state screen). We then organize all sgRNAs into tiers (y-axis, tiers one through four) based on the percent of single guide RNAs against a target showing at least a two-fold change in representation on $NGFR^{HIGH}$/$EGFR^{HIGH}$ cells. In red, we labeled targets that when tested again produced at least a 50% change in the frequency of $NGFR^{HIGH}$ cells. In black, we labeled targets that we tested but did not validate, and in gray we show targets we did not test. We display the percent of genes tested and validated at each tier on the right.

Supplemental Figure 9. Percent of targets from the fate screen that validate.
To assess the sensitivity of our screen, we validated the effect observed in the initial fate screen for a select group of targets via colony formation assays. Here, each dot represents an individual single guide RNA, and we plot the change in single guide RNA representation between cells resistant to vemurafenib and cells that have never been exposed to the drug (as measured in the fate screen). We then organize all single guide RNAs into tiers (y-axis, tiers one through four) based on the percent of single guide RNAs against a target showing at least a two-fold change in representation on drug resistant cells. In red, we labeled targets that when tested again produced at least a 50% change in the frequency colonies resistant to $BRAF^{V600E}$ inhibition. In black, we labeled targets that we tested but did not validate, and in gray we show targets we did not test. We display the percent of genes tested and validated at each tier on the right.

Supplemental Figure 10. Transcriptional effects induced by knockout of select screen targets.

A. The heatmap represents the biclustering analysis of different screen targets (rows) based on the change in expression of all genes differentially expressed in at least one knockout (columns). Within the heatmap, red indicates an increase in expression following the knockout, while blue indicates a decrease in gene expression (see heatmap color key). Each target (rows) represents transcriptomes of biological triplicates (unless otherwise stated on Supplemental Table 4). Target labels (rows) in green indicate genes whose knockout increased the frequency of $NGFR^{HIGH}/EGFR^{HIGH}$ cells in the initial screen. In red are those whose knockout increased the number of cells resistant to vemurafenib, and in gray are those that decreased the frequency of either $NGFR^{HIGH}/EGFR^{HIGH}$ cell or of cells resistant to vemurafenib. As before, we organized targets into confidence tiers indicated by the number of asterisks, based on the percent of single guide RNAs against that target that showed an effect in the initial screen (see knockout color key).

B. We performed principal component analysis of the transcriptional effects induced by the knockout of select screen targets. We used as input the gene set enrichment scores from Fig. 3A to identify primary axes that account for the greatest degree of transcriptome variability across knockout cell lines. The color indicates the effect of the knockout in the initial state screen. The size of the dot indicates the degree of confidence we have in each particular hit based on the percent of the single guide RNAs against a target that passed a threshold of two-fold change in the initial state screen. In black, we labeled melanoma cells where we did not knockout any targets but either enriched for $EGFR^{HIGH}$ cells, $NGFR^{HIGH}$ cells, $EGFR^{HIGH}/NGFR^{HIGH}$ cells, or for cells resistant to vemurafenib.

Supplemental Figure 11. Technical validation of WM989-A6-G3-Cas9-5a3 cell line.

A. WM989-A6-G3-Cas9-5a3 cells expressing NGFR, EGFR, and both NGFR and EGFR are more likely to survive and proliferate in the presence of vemurafenib (*14*). Here, we show the number of colonies that grow upon vemurafenib exposure in a mixed population of WM989-A6-G3-Cas9-5a3 or in the same population but enriched for $EGFR^{HIGH}$ cells, $NGFR^{HIGH}$ cells, or $NGFR^{HIGH}/EGFR^{HIGH}$ cells.

B. In this plot, we show the single guide RNA representation (as percent GFP-positive cells) of controls over time in WM989-A6-G3 cells with or without Cas9 expression. Negative controls (black) are single guide RNAs aimed at ROSA26, a non-expressing gene in human melanoma. Positive controls (red) target proteins necessary for cell viability. Only cells expressing both Cas9 and a positive control single guide RNA should disappear from the population over time.

Supplemental Tables

All tables can be found at:
https://www.dropbox.com/sh/t08558cl4mepfm6/AABBvbtlTPSNNPoMC9NTro-9a?dl=0

Figure 1

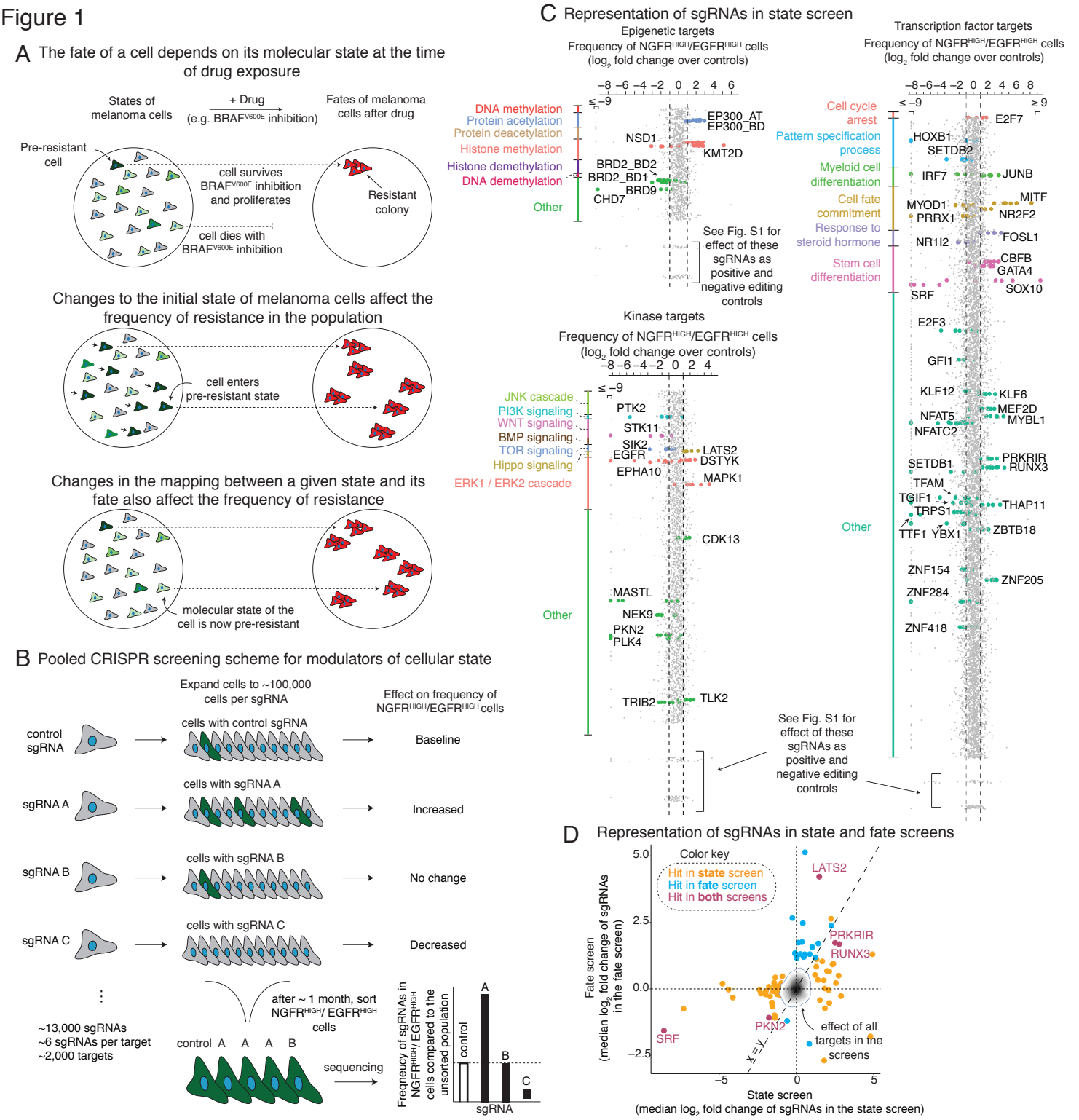

Figure 1. Pooled CRISPR screen design to identify modulators of cellular plasticity in the context of drug resistance to targeted therapies in melanoma.

A. (top) In melanoma, the initial molecular profile (i.e., "state") of a cell within an otherwise homogeneous population, indicated by green vs. gray coloring of cell, dictates the ultimate fate of the cell (e.g. proliferation vs. death). Changing the number of cells in a given state (A, middle) or the mapping between state and fate (A, bottom) can alter the number of resistant colonies that form upon addition of the $BRAF^{V600E}$ inhibitor vemurafenib.

B. We designed a pooled CRISPR screen to detect modulators of the rare cellular states that lead to drug resistance. After transducing a library of single guide RNAs and expanding the population, we isolated cells with high expression of both NGFR and EGFR, then sequenced the single guide RNAs to determine which gene knockouts alter the frequency of these cells. Changes in the frequency of a given single guide RNA in this population (e.g. targets A and C) indicate that these targets may affect the frequency of $NGFR^{HIGH}/EGFR^{HIGH}$ cells in the population, and thus may affect the cellular state associated with pre-resistance.

C. After transducing a population of melanoma cells and isolating $NGFR^{HIGH}/EGFR^{HIGH}$ cells (see Fig. 1B), we quantified the frequency of each single guide RNA in the resulting population. Our screening scheme utilized three separate pooled single guide RNA libraries, one targeting epigenetic domains (top left), another targeting kinases (bottom left), and a final one targeting transcription factors (right). We organized the targets within each single guide RNA library by biological process. (While a given target could fall into several categories, each target is assigned to a single group and plotted only once.) Each dot represents a single guide RNA, grouped by gene target (5-6 single guide RNAs per target), with the $\log_2$ fold change representing the number of times the single guide RNA was detected in the sorted population versus an unsorted population of melanoma cells transduced with the same library. For display purposes, all single guide RNAs with fold changes beyond the axis limits were placed at the edge of the axis as indicated. For targets considered "hits" by our rubric (see methods), we labeled the single guide RNA dot by the color assigned to that biological process. Dots at the bottom of each pane correspond to non-targeting controls (single guide RNAs not targeting any loci in the genome) and cell viability controls (e.g. proteins required for cell survival and proliferation, but not specifically associated with rare-cell behavior). Supplemental Fig. 1 provides details on the effect of these editing controls.

D. Effect overlap between state and fate hits. Each target's position (dots) represents the number of times (as median $\log_2$ fold change) the single guide RNAs were detected in the $NGFR^{HIGH}/EGFR^{HIGH}$ population vs. an unsorted population of melanoma cells (state screen, x-axis), or in the population of cells resistant to vemurafenib vs. the population of cells prior to treatment (fate screen, y-axis). Orange labels correspond to high confidence targets (Tier 1 and Tier 2) in the state screen; blue corresponds to high confidence targets in the fate screen; purple corresponds to high confidence targets in both screens. The effects of all targets in both screens are displayed as a density histogram.

Figure 2

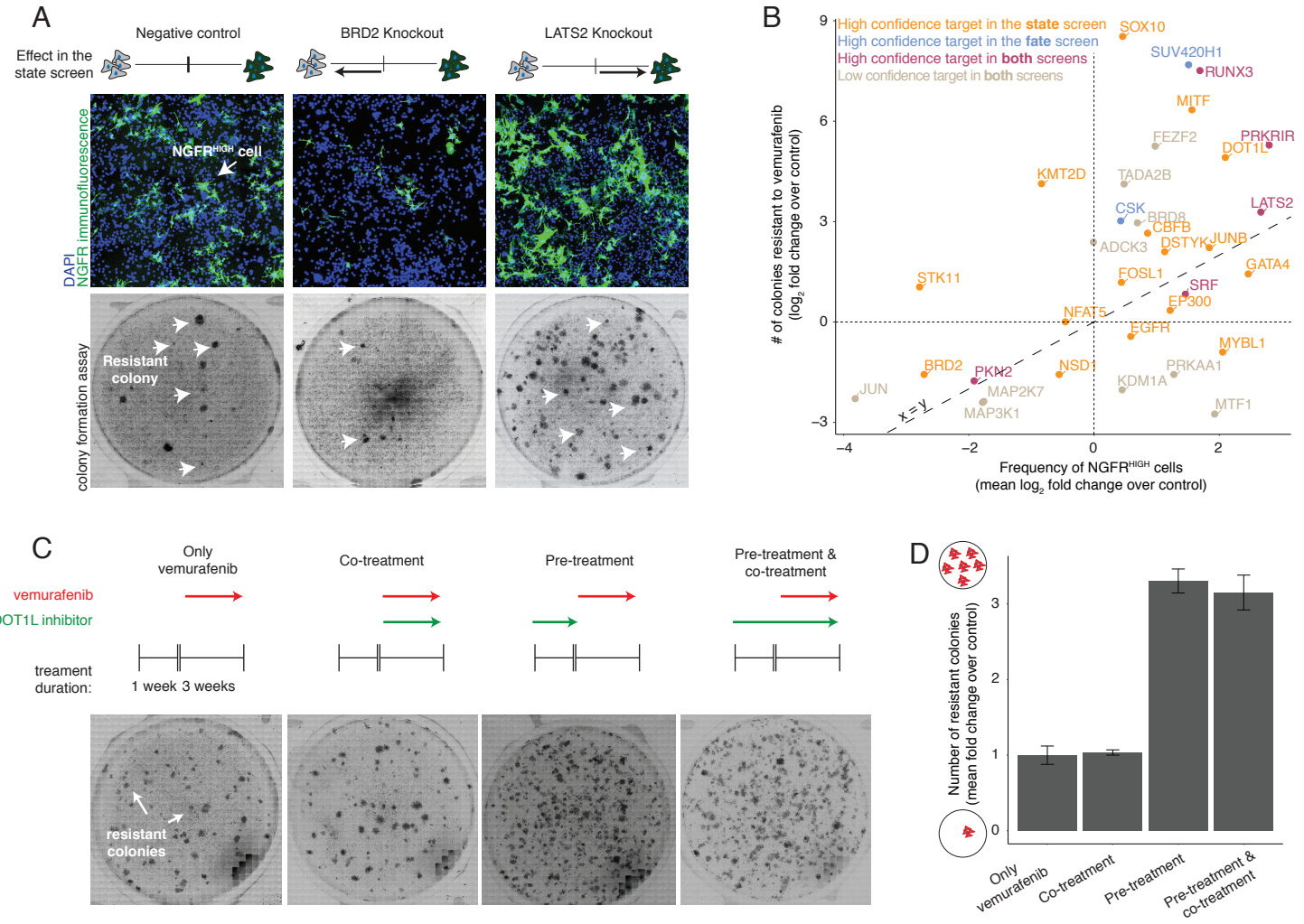

Figure 2. Effects of variability hits on resistant colony formation.

A. To validate the phenotypic effect of targets identified by our genetic screen, we knocked out 83 of the targets and quantified both the frequency of NGFR^{HIGH} cells by immunofluorescence using anti-NGFR antibodies (top) and the number of resistant colonies (bottom) that form upon BRAF^{V600E} inhibition. Here we show example state and fate validation of BRD2 and LATS2 knockouts. The schematic represents the effect of the knockout in the state screen on the frequency of NGFR^{HIGH}/EGFR^{HIGH} cells.

B. Relationship between the frequency of NGFR^{HIGH} cells (x-axis) and the number of resistant colonies (y-axis). We plot the frequency of NGFR^{HIGH} cells as the mean $\log_2$ fold change over three replicates in the number of NGFR^{HIGH} cells following knockout of the gene indicated, normalized by cells with non-targeting sgRNAs. (For variability of the effect size across replicates of a given target, see Supplemental Fig. 5). We quantified the $\log_2$ fold change in the number of resistant colonies in the knockout cell line as compared to the non-targeting control cell lines. Orange points are targets identified as high confidence hits (Tier 1 and Tier 2) in the state screen; blue are those identified as high confidence hits in the fate screen; purple are those identified as high confidence hits in both state and fate screen; gray, those that may have shown an effect in either or both screens, but were not classified as high confidence hits in either screen.

C. To assess the effect of DOT1L inhibition (green arrows, pinometostat at 4μM) at different times on a cell's ability to survive BRAF^{V600E} inhibition, we first established a baseline number of colonies that grow when WM989-A6-G3 cells are exposed to 1μM of vemurafenib for three weeks (leftmost panel). Then, in a separate population, we either inhibited BRAF^{V600E} and DOT1L simultaneously (co-treatment), inhibited DOT1L first (seven days) and then BRAF^{V600E} (three additional weeks; pre-treatment), or inhibited DOT1L before (seven days) and during three weeks of vemurafenib treatment (pre-treatment and co-treatment).

D. Number of resistant colonies that result from each therapeutic regimen in Fig. 2C as the mean fold change over baseline (vemurafenib alone) for three replicates normalized to the number of cells in culture prior to BRAF^{V600E} inhibition. Error bars indicate the standard error of the mean over triplicates.

Figure 3

A Gene set enrichment analysis of GO Term gene sets (Biological process)

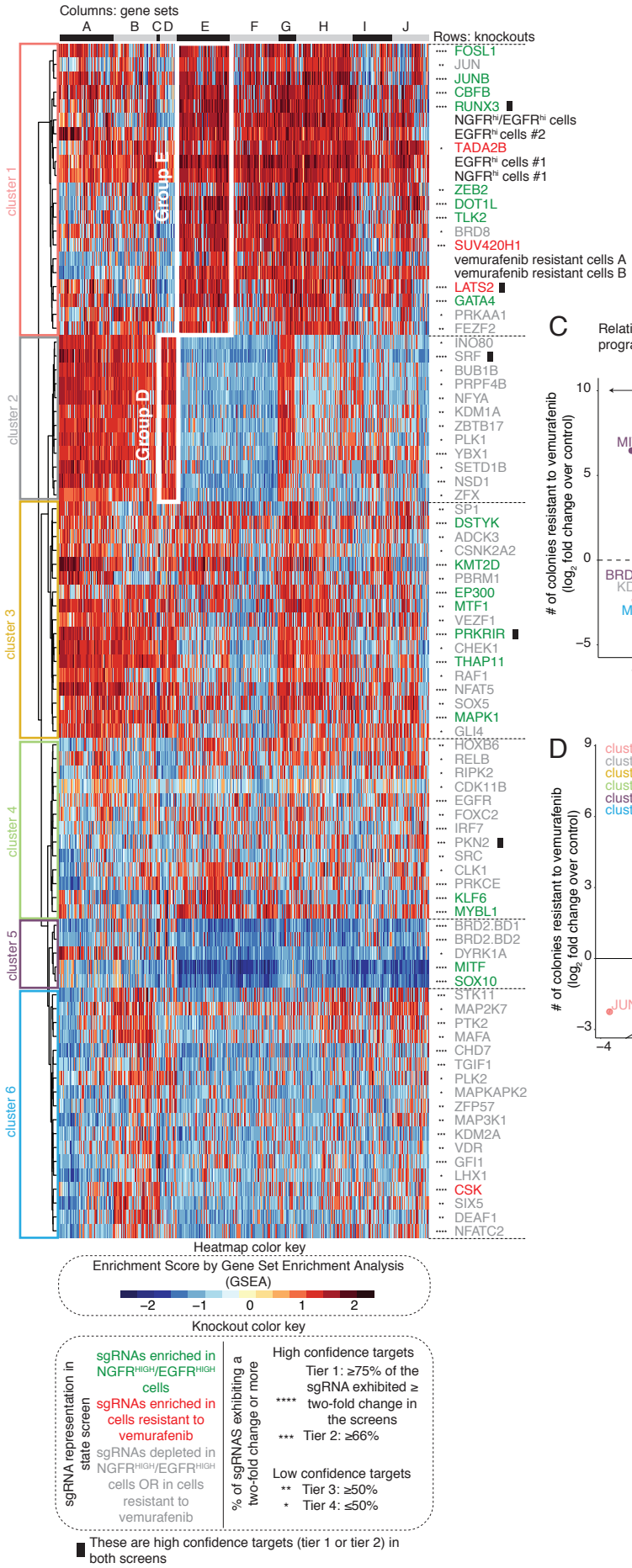

B Select list of gene sets in:

Group E	Group D
Neural crest cell differentiation	Amino acid biosynthetic process
Melanocyte differentiation	Regulation of mRNA metabolic process
Neural crest cell migration	Fatty Acyl Co-A metabolic process
Regulation of cell matrix adhesion	Nucleotide base excision repair
Regulation of chemotaxis	
Regulation of MAPK cascade	
Angiogenesis	
Hippo signaling	
Cell fate specification	

See supplemental table 6 for full list of gene sets

C Relationship between expression of differentiation programs and resistance to vemurafenib

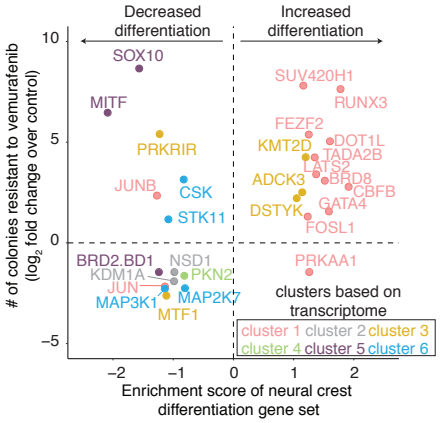

D

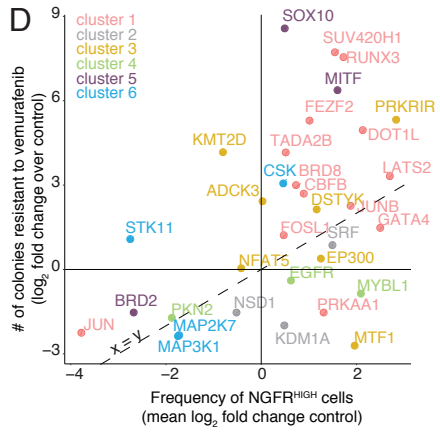

Figure 3. Gene set enrichment analysis of the transcriptional effects induced by the knockout of select screen targets.

A. The heatmap represents biclustering analysis of different knockout cell lines (rows) based on the Gene Set Enrichment Analysis score of Gene Ontology gene sets (Biological process GO terms, columns in heatmap). Within the heatmap, red indicates enrichment in the sense that there are more differentially upregulated genes in knockout vs. control in that gene set than expected by chance, whereas blue indicates enrichment of downregulated genes (shade indicates degree of enrichment). Each target knockout (rows) represents transcriptomes of biological triplicates (unless otherwise stated on Supplemental Table 4). Target labels (rows) in green indicate genes whose knockout increased the frequency of NGFR^{HIGH}/EGFR^{HIGH} cells in the screen, while red indicates targets whose knockout increased the number of cells resistant to vemurafenib, and gray indicates targets that decreased the frequency of either NGFR^{HIGH}/EGFR^{HIGH} cells or of cells resistant to vemurafenib. As before, we organized targets into high confidence hits (Tier 1 and Tier 2) and low confidence hits (Tiers 3 and Tier 4) based on the percentage of single guide RNAs against a target that showed at least a two-fold change in the initial screen (see knockout color key).The asterisks next to the label indicate the tier (Tier 1, ****; Tier 2, ***; Tier 3, **; Tier 4, *). Based on the dendrogram on the left, we grouped targets into six clusters. We also clustered gene sets (columns) into groups, labeled by the letters on top of the heatmap. The white boxes inside the heatmap demark groups of gene sets specifically upregulated in a given cluster.

B. Select list of gene sets in groups D and E from Fig. 3A. For a complete list of gene sets within each group, see supplementary table 6.

C. Relationship between the expression of genes involved in neural crest differentiation (x-axis) and the number of colonies resistant to vemurafenib (y-axis) following the knockout of a target. For each knockout, we plot the expression of neural crest differentiation genes as the enrichment score obtained through gene set enrichment analysis for the neural crest differentiation gene set (GO term). We quantified the $\log_2$(fold change) in the number of resistant colonies in the knockout cell line as compared to the non-targeting control cell lines. Colors represent the cluster grouping of each knockout based on Fig. 3A.

D. Relationship between the frequency of NGFR^{HIGH} cells (x-axis) and the number of resistant colonies (y-axis). As in Fig. 2B, we plot the frequency of NGFR^{HIGH} cells as the median $\log_2$(fold change) over three replicates in the number of NGFR^{HIGH} cells following knockout of the indicated gene normalized by cells with non-targeting single guide RNAs. (For variability of the effect size across replicates of a given target, see Supplemental Fig. 5.) We quantified the $\log_2$(fold change) in the number of resistant colonies in the knockout cell line as compared to the non-targeting control cell lines. We color-coded all targets by groupings based on their transcriptomes (see Fig. 3A) following knockout of the gene indicated.

Figure 4

The number of pre-resistant cells beyond a population's adaptation threshold determines the number of cells that survive the drug

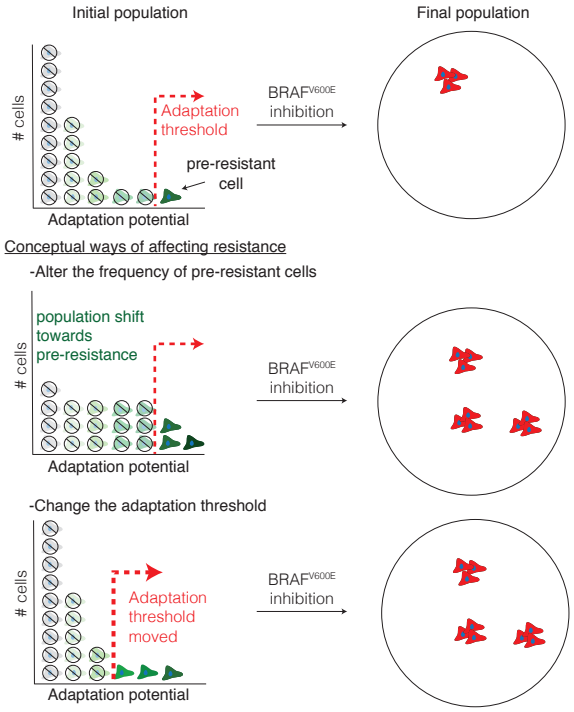

Figure 4. Model of adaptation thresholds and cellular heterogeneity in the development of resistance to targeted therapies. Variability in the expression of various markers are associated with an individual cell's probability to survive drug treatment. In one simple model, cellular variability occurs along a single ordinate, which can be conceptualized as the degree of "greenness". Operationally, this may be related to the expression of a marker of pre-resistance, such as NGFR. In this model, there is a threshold (red line, top panel) that divides cells along this axis into those that adapt to the drug and become resistant vs. those that no longer proliferate when challenged with drug. Here, there are at least two ways by which one could conceivably alter the number of cells that survive the drug. In one scenario (middle) the distribution of "greenness" could change, leading to more cells being above the threshold, leading to more resistant colonies. In another scenario, the distribution of phenotypes remains unchanged, but the threshold itself moves, also leading to more resistant colonies. Our results suggest (but do not prove) that both scenarios may play out to varying degrees as a result of different genes being knocked out.

Supplemental Figure 1

A Change in sgRNA representation of negative and positive controls

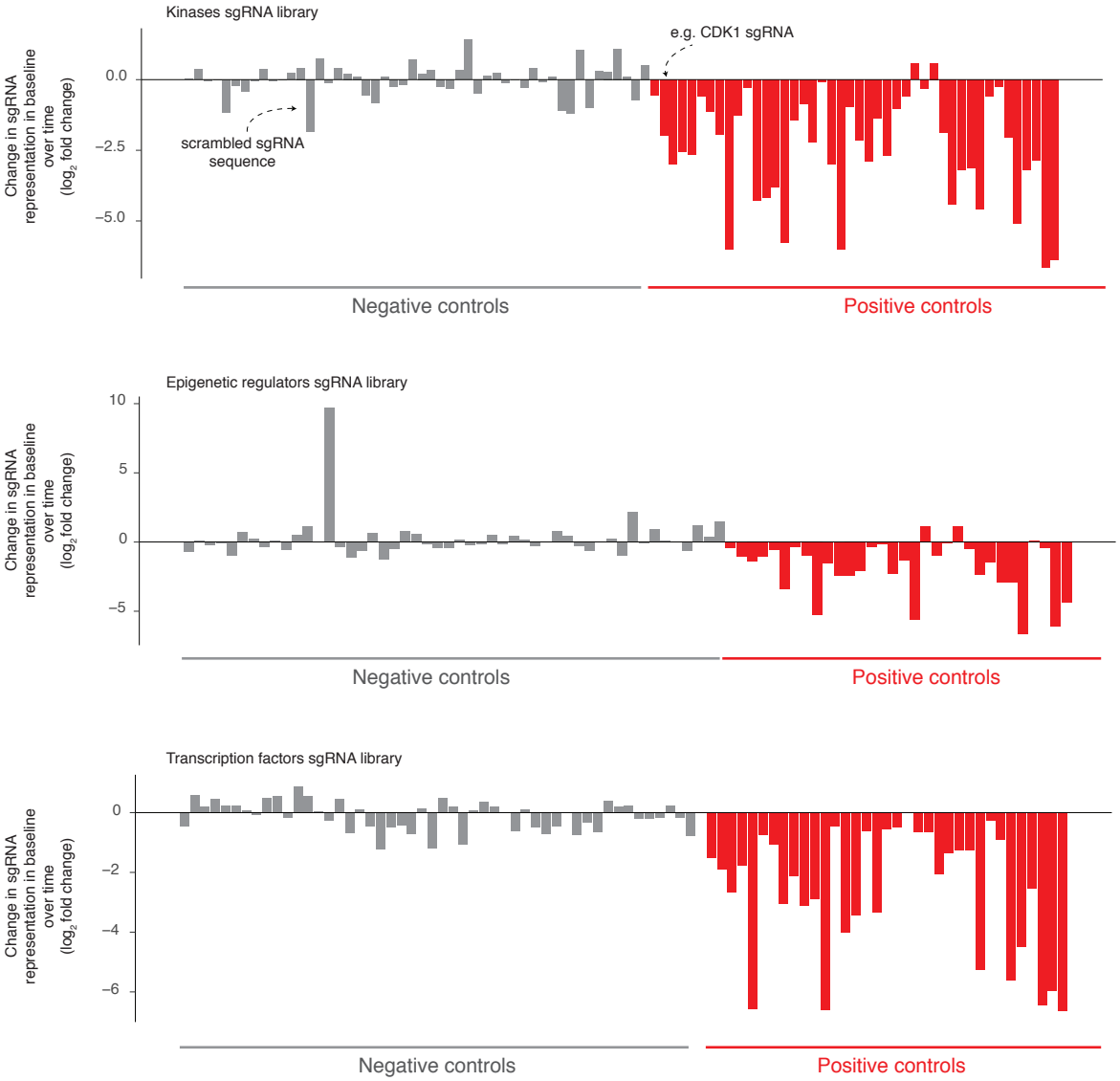

Supplemental Figure 1. Effect of negative and positive control single guide RNAs in the CRISPR screens. Our pooled CRISPR screen included non-targeting single guide RNAs as negative controls (gray bars, 50+ single guide RNAs) as well as single guide RNAs affecting cell viability as positive controls (red bars, 25+ single guide RNAs). We quantified the change in representation of these single guide RNAs over time and report the log_2 fold change in representation from six days after transfection to right before selection (vemurafenib exposure or selection by NGFR and EGFR expression). We expect positive controls to lose representation over time more often than negative controls. Our screening scheme utilized three separate pooled single guide RNA libraries, one targeting kinases (top), another targeting epigenetic domains (middle), and a final one targeting transcription factors (bottom).

Supplemental Figure 2

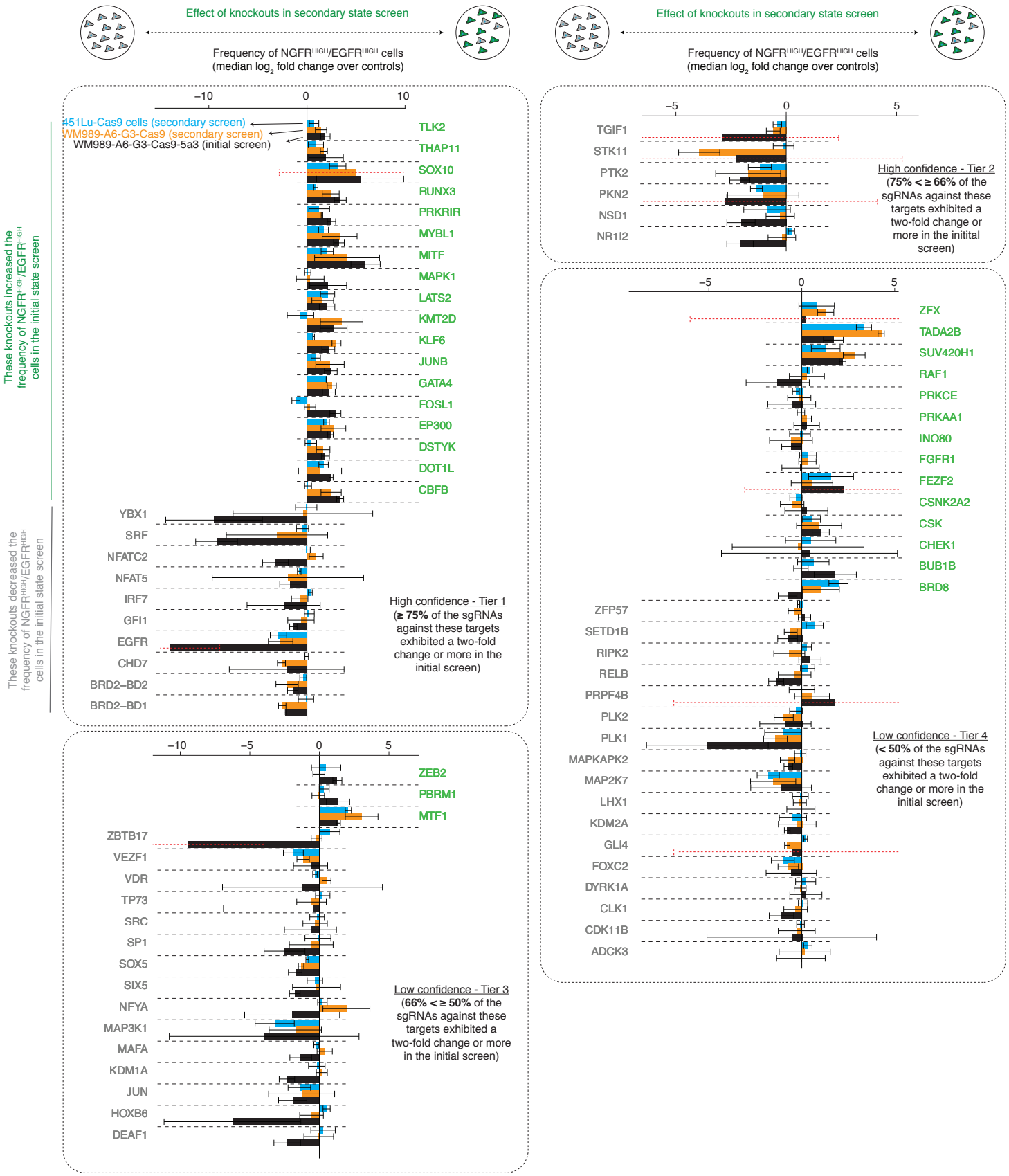

Supplemental Figure 2. Secondary validation of hits across multiple cell lines by secondary targeted CRISPR screening. We assessed the robustness and generality of the effect of hits identified in the state screen (WM989-A6-G3-Cas9-5a3, black bars) by carrying out a secondary screen containing single guide RNAs for 34 of the high confidence hits (Tiers 1 and 2) we identified in the state screen, as well as another 52 lower confidence factors from Tiers 3 and 4 (these lower confidence hits may also have been high confidence hits in the "fate" screen). See Supplemental Table 5 for a list of the targets. We carried out this screen in WM989-A6-G3-Cas9 (orange bars) as well as in another BRAF^{V600E} melanoma cell line (451Lu-Cas9, blue). Within each tier, names labeled in green correspond to targets whose single guide RNAs are enriched in NGFR^{HIGH}/EGFR^{HIGH} cells in the initial screen and gray represents targets whose single guide RNAs are underrepresented in these rare cells. We plotted the median $\log_2$ fold change in single guide RNA representation (normalized by non-targeting controls) across three single guide RNAs. Error bars represent the standard deviation of the fold change across all single guide RNAs for a given target. Dotted error bars in red extend beyond the limits of the graph. Note that the limits of the axes vary between tiers. We found that 25 of the 34 high confidence hits showed at least a two fold change in the frequency of NGFR^{HIGH}/EGFR^{HIGH} cells concordant with the effects detected in the original screening clonal cell line (WM989-A6-G3-Cas9-5a3). In 451Lu-Cas9 cells, 20 of the 34 targets also showed a change in the frequency of NGFR^{HIGH}/EGFR^{HIGH} cells, with 11 of those exhibiting at least a two-fold change. Although quantitatively they were not as strong as the effects of the Tier 1 and 2 hits, even Tier 3 and 4 hits displayed qualitative agreement in these secondary screens.

Supplemental Figure 3

A

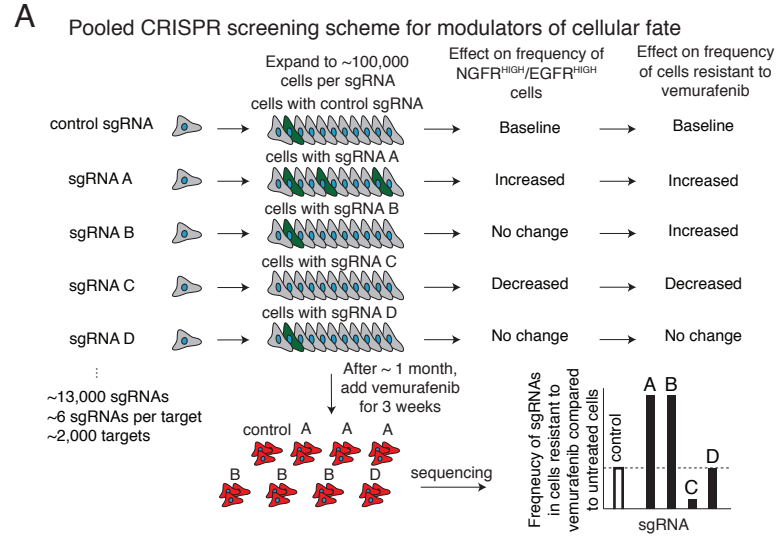

Supplemental Figure 3. Screen for factors modulating number of resistant colonies upon BRAFV600E inhibition (cellular "fate").
A. We performed a pooled CRISPR screen to detect modulators of cellular fate (e.g. number of drug-resistant colonies) in the presence of the $BRAF^{V600E}$ inhibitor vemurafenib. After transducing a library of single guide RNAs and expanding the population, we exposed the cells to the $BRAF^{V600E}$ inhibitor vemurafenib (1μM) for 3 weeks, after which we sequenced the single guide RNAs in the surviving population. Changes in the frequency of detection of a given single guide RNA indicates that its target may affect the ability of a cell to survive and proliferate upon $BRAF^{V600E}$ inhibition.
B. After transfecting a population of melanoma cells, we exposed them to vemurafenib ($BRAF^{V600E}$ inhibitor, 1μM) for three weeks to grow resistant colonies. We then sequenced the DNA to quantify the single guide RNA representation of each target in the resulting population, using the same libraries as in Fig. 2. As before, we ranked the targets into tiers based on the percent of single guide RNAs that exhibited at least a two-fold change in representation throughout the screen (Tier 1, ≥ 75%; Tier 2, ≥ 66%; Tier 3, ≥ 50%; Tier 4, < 50%), thus reflecting the degree of confidence we have in the hit (High confidence hits: Tiers 1 and 2; Low confidence hits: Tiers 3 and 4). In this screen, we identified 24 high confidence factors. For a more detailed description see the methods section.

B

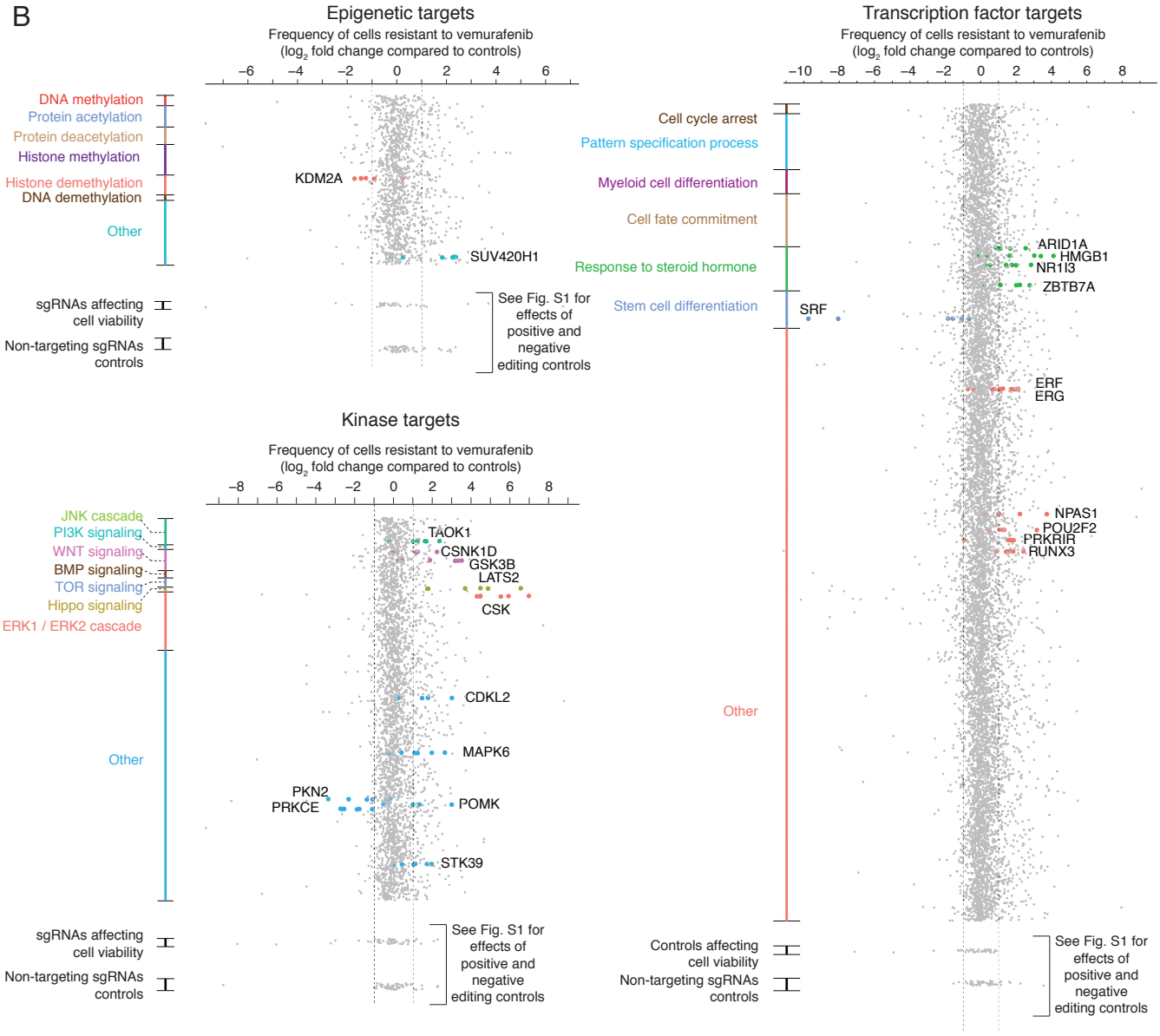

Supplemental Figure 4

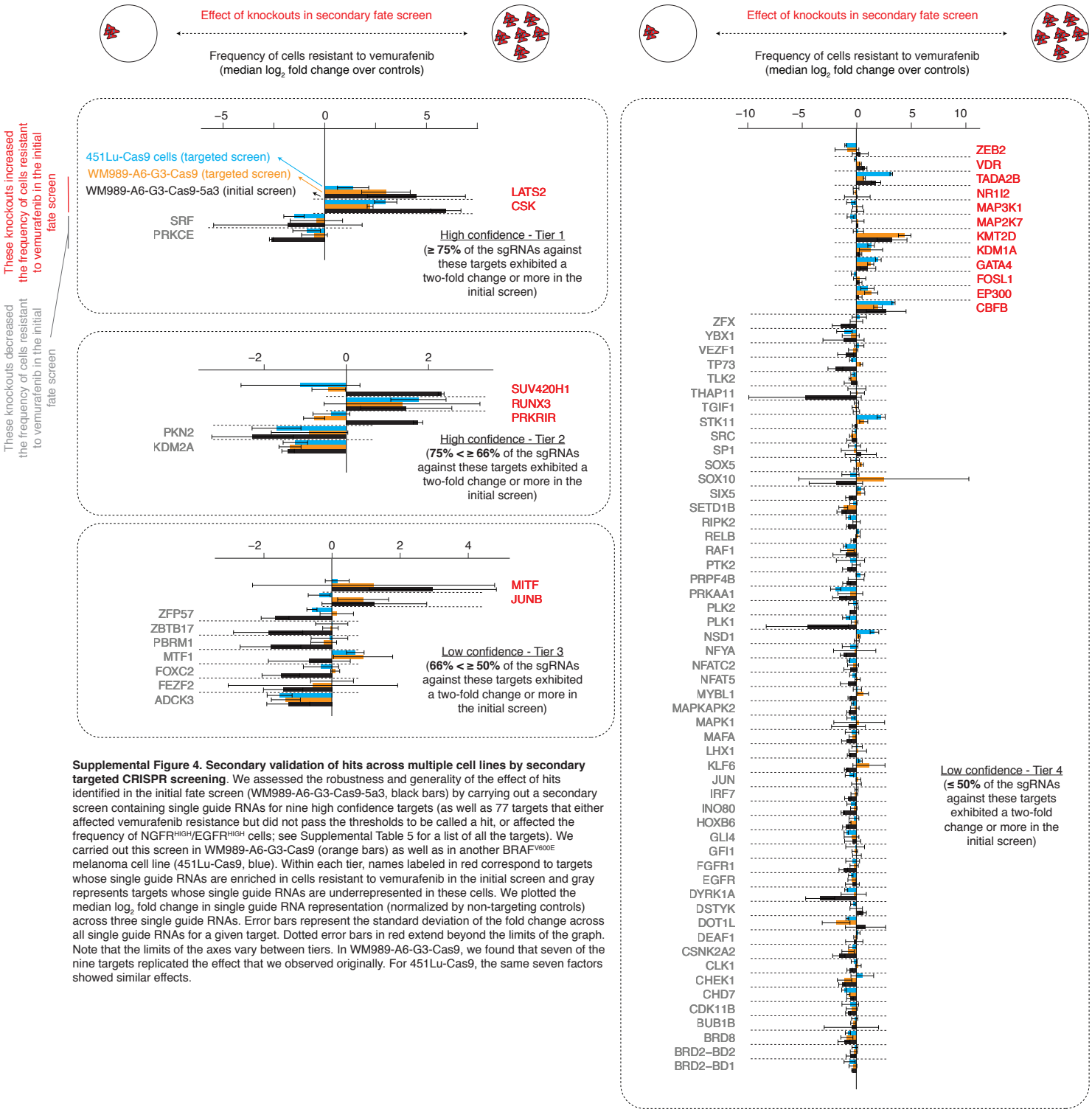

Supplemental Figure 4. Secondary validation of hits across multiple cell lines by secondary targeted CRISPR screening. We assessed the robustness and generality of the effect of hits identified in the initial fate screen (WM989-A6-G3-Cas9-5a3, black bars) by carrying out a secondary screen containing single guide RNAs for nine high confidence targets (as well as 77 targets that either affected vemurafenib resistance but did not pass the thresholds to be called a hit, or affected the frequency of NGFR^{HIGH}/EGFR^{HIGH} cells; see Supplemental Table 5 for a list of all the targets). We carried out this screen in WM989-A6-G3-Cas9 (orange bars) as well as in another BRAF^{V600E} melanoma cell line (451Lu-Cas9, blue). Within each tier, names labeled in red correspond to targets whose single guide RNAs are enriched in cells resistant to vemurafenib in the initial screen and gray represents targets whose single guide RNAs are underrepresented in these cells. We plotted the median $\log_2$ fold change in single guide RNA representation (normalized by non-targeting controls) across three single guide RNAs. Error bars represent the standard deviation of the fold change across all single guide RNAs for a given target. Dotted error bars in red extend beyond the limits of the graph. Note that the limits of the axes vary between tiers. In WM989-A6-G3-Cas9, we found that seven of the nine targets replicated the effect that we observed originally. For 451Lu-Cas9, the same seven factors showed similar effects.

Supplemental Figure 5

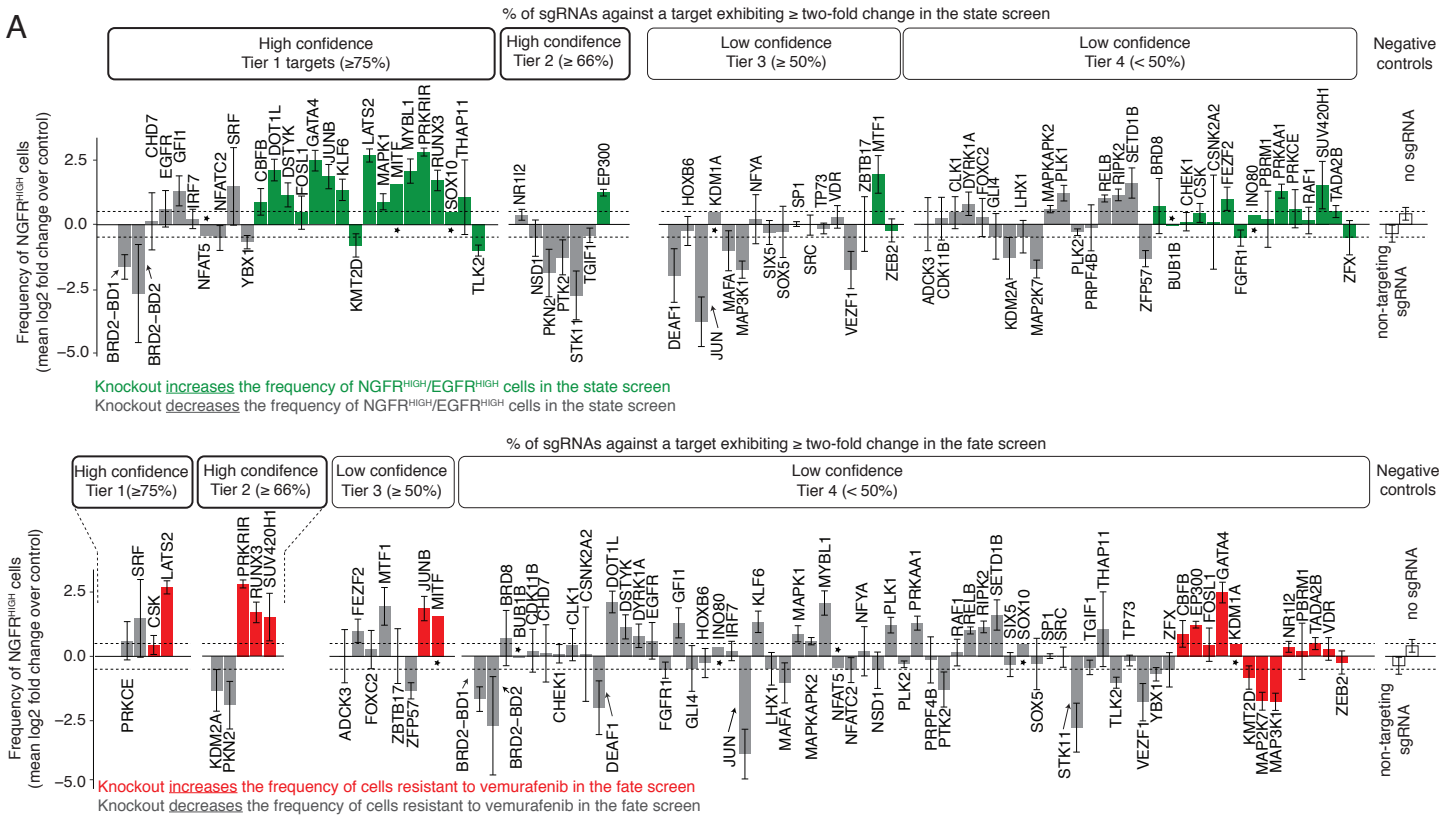

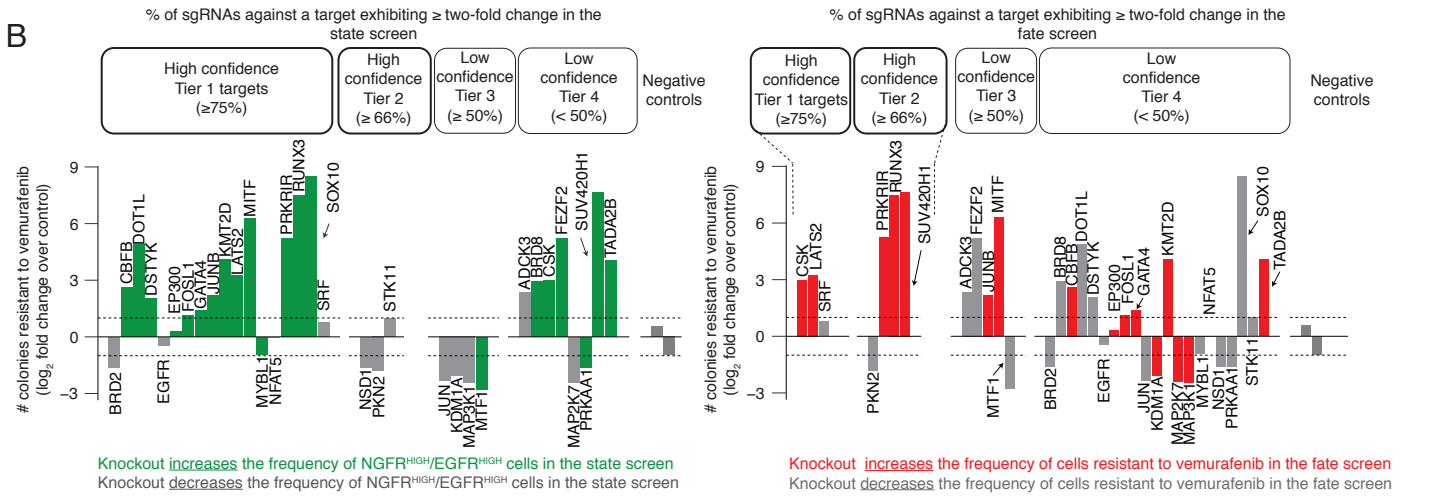

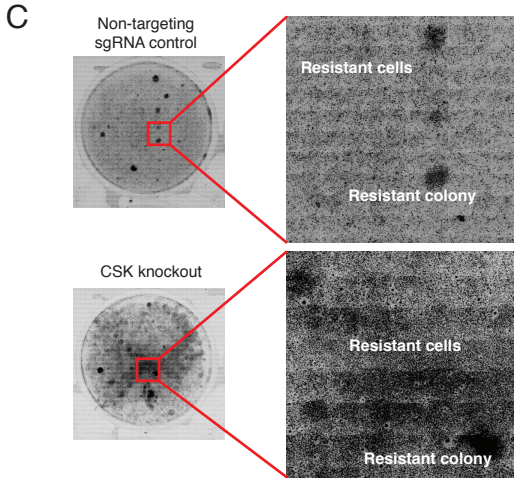

Supplemental Figure 5. Validation of effects on state and fate of variability hits by via NGFR immunofluorescence and resistant colony formation.

A. Frequency of NGFR^{HIGH} cells following the knockout of select targets. Each bar represents the change in the number of NGFR^{HIGH} cells following knockout of the gene indicated over replicates, each using a different single guide RNA. Error bars represent the standard error of the mean across the replicates. We carried out each measurement over three replicates, but excluded samples with low cell density (< 500 cells). The star above or below the bars indicate targets where, after excluding samples with low cell numbers, n = 1. Tier refers to the degree of confidence we have in each particular hit, with tier 1 representing highest confidence hits for which ≥ 75% of the single guide RNAs passed a threshold of two-fold change in the initial state screen. We performed this analysis for hits from both the state screen (top) and the fate screen (bottom). 21 of 34 high confidence hits from the state screen showed at least a 50% increase or decrease in the frequency of NGFR^{HIGH} cells over control. Of the lower confidence hits (Tier 3 and Tier 4) 21 out of 49 targets increased or decreased the frequency of NGFR^{HIGH} cells by 50% or more.

B. Resistance phenotype of melanoma cells following the knockout of hits from the initial screens. Each bar represents the $\log_2$ fold change over non-targeting control in the number colonies able to grow in vemurafenib following knockout of the gene indicated. The number of colonies for each target is normalized to the number of cells present in culture before BRAF^{V600E} inhibition, reported as number of colonies per every 10,000 cells in culture prior to treatment (see methods). As before, the different tiers represent the percent of single guide RNAs against a given target exhibiting at least a two-fold change throughout the initial (left) state or (right) fate screens. On the left panel, we label in green and gray the effect a given target has in the frequency of NGFR^{HIGH}/EGFR^{HIGH} cells (based on the initial state screen). On the right panel, we label in red and gray the effect a given target has in the number of cells that resist BRAF^{V600E} inhibition (based on the initial fate screen). In this plot, each bar represents one experimental replicate. See Supplemental Fig. 6 for replicates.

C. These images show the effect of CSK knockout on a cell's ability to develop resistance to BRAF^{V600E} inhibition. Here, we plated CSK-knockout WM989-A6-G3-Cas9-5a3 cells and exposed them to 1μM vemurafenib for three weeks. As before, after the treatment we counted the number of resulting colonies and compared it to the number of colonies resulting from WM989-A6-G3-Cas9-5a3 cells without the knockout. Note that the number of resistant cells in the CSK sample is too large to accurately identify individual colonies. We only counted colonies we could clearly delineate, and thus, the number of colonies reported is an underestimate.

Supplemental Figure 6

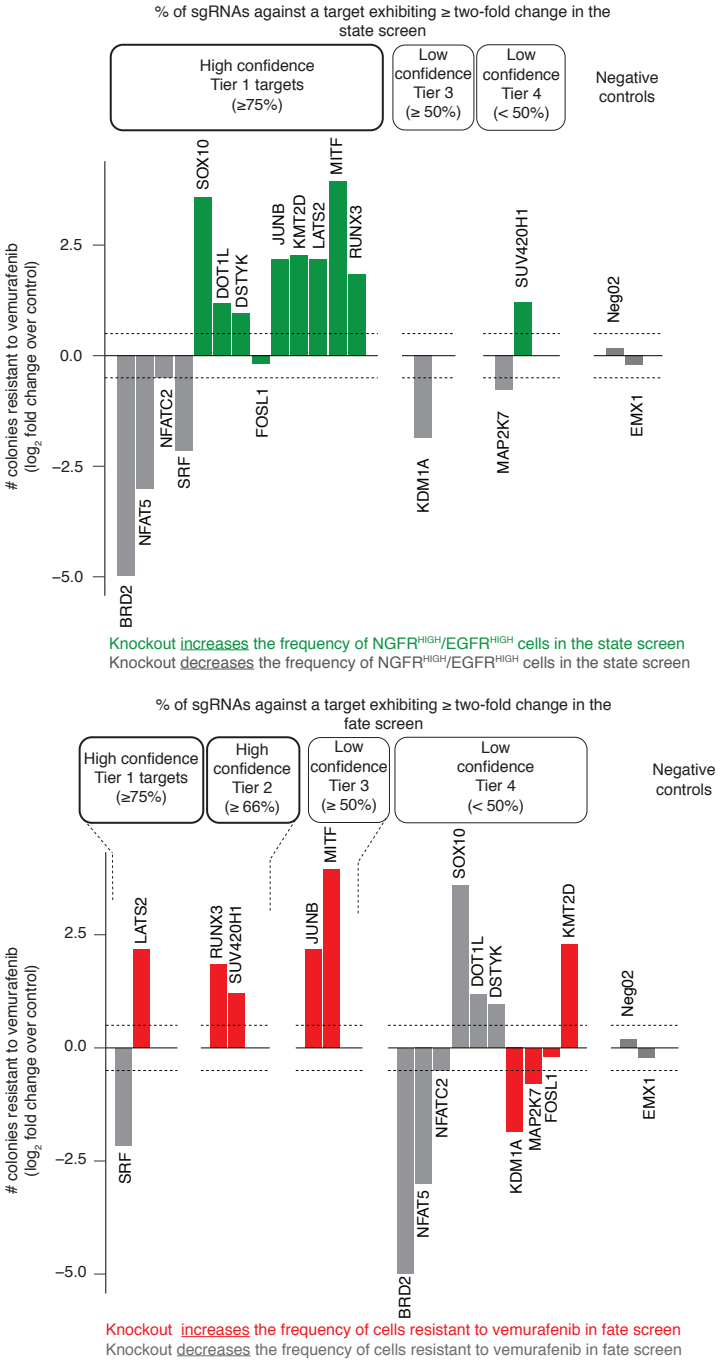

Supplemental Figure 6. Validation of effects on fate of variability hits by resistant colony formation. Resistance phenotype of melanoma cells following the knockout of hits from the initial screens. Each bar represents the $\log_2$ fold change over non-targeting control in the number of colonies able to grow following knockout of the gene indicated. The number of colonies for each target is normalized to the number of cells present in culture before $BRAF^{V600E}$ inhibition, reported as number of colonies per every 10,000 pre-treatment cells (see methods). As before, the different tiers represent the percent of single guide RNAs against a given target exhibiting at least a two-fold change throughout the (top) state or (bottom) fate screens. On the top panel, we labeled in green and gray the effect a given target has in the frequency of $NGFR^{HIGH}/EGFR^{HIGH}$ cells (based on the state screen). On the bottom panel, we labeled in red and gray the effect a given target has in the number of cells that resist $BRAF^{V600E}$ inhibition (based on the fate screen). In this plot, each bar represents one experimental replicate (distinct from the one in Supplemental Fig. 5B).

Supplemental Figure 7

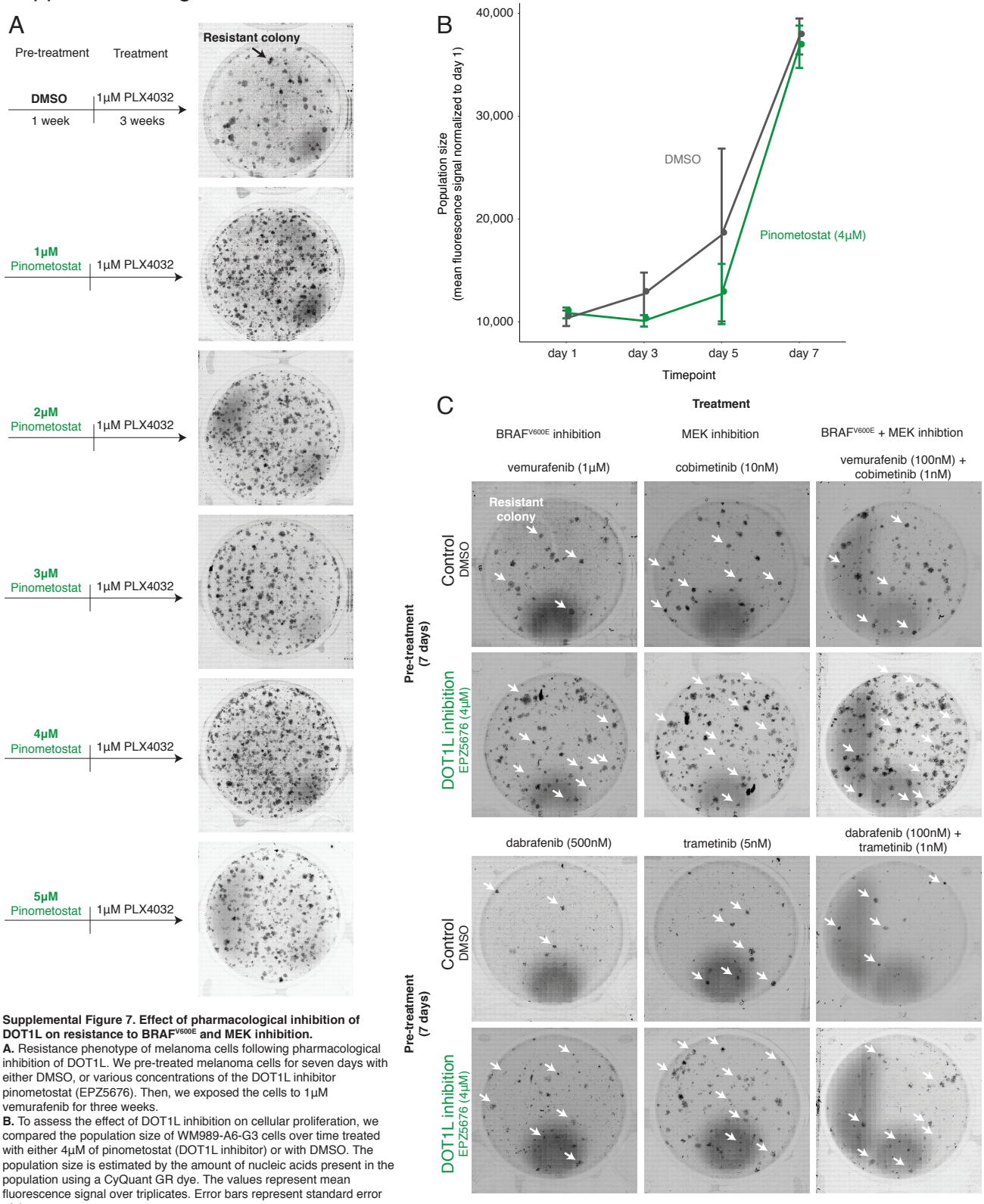

Supplemental Figure 7. Effect of pharmacological inhibition of DOT1L on resistance to BRAF^{V600E} and MEK inhibition.
A. Resistance phenotype of melanoma cells following pharmacological inhibition of DOT1L. We pre-treated melanoma cells for seven days with either DMSO, or various concentrations of the DOT1L inhibitor pinometostat (EPZ5676). Then, we exposed the cells to 1μM vemurafenib for three weeks.
B. To assess the effect of DOT1L inhibition on cellular proliferation, we compared the population size of WM989-A6-G3 cells over time treated with either 4μM of pinometostat (DOT1L inhibitor) or with DMSO. The population size is estimated by the amount of nucleic acids present in the population using a CyQuant GR dye. The values represent mean fluorescence signal over triplicates. Error bars represent standard error of the mean.
C. Resistance phenotype of melanoma cells to BRAF^{V600E} and MEK inhibitors following pharmacological inhibition of DOT1L. We pre-treated melanoma cells for seven days with either DMSO or 4μM of pinometostat. We then exposed the cells to one of two BRAF^{V600E} inhibitors (vemurafenib and dabrafenib, left panels), to one of two MEK inhibitors (cobimetinib and trametinib, middle panels), or to a combination of a BRAF^{V600E} and MEK inhibitor (vemurafenib + cobimetinib; dabrafenib + trametinib, right panels). White arrows point to a few of the many colonies that grew under each condition.

Supplemental Figure 8

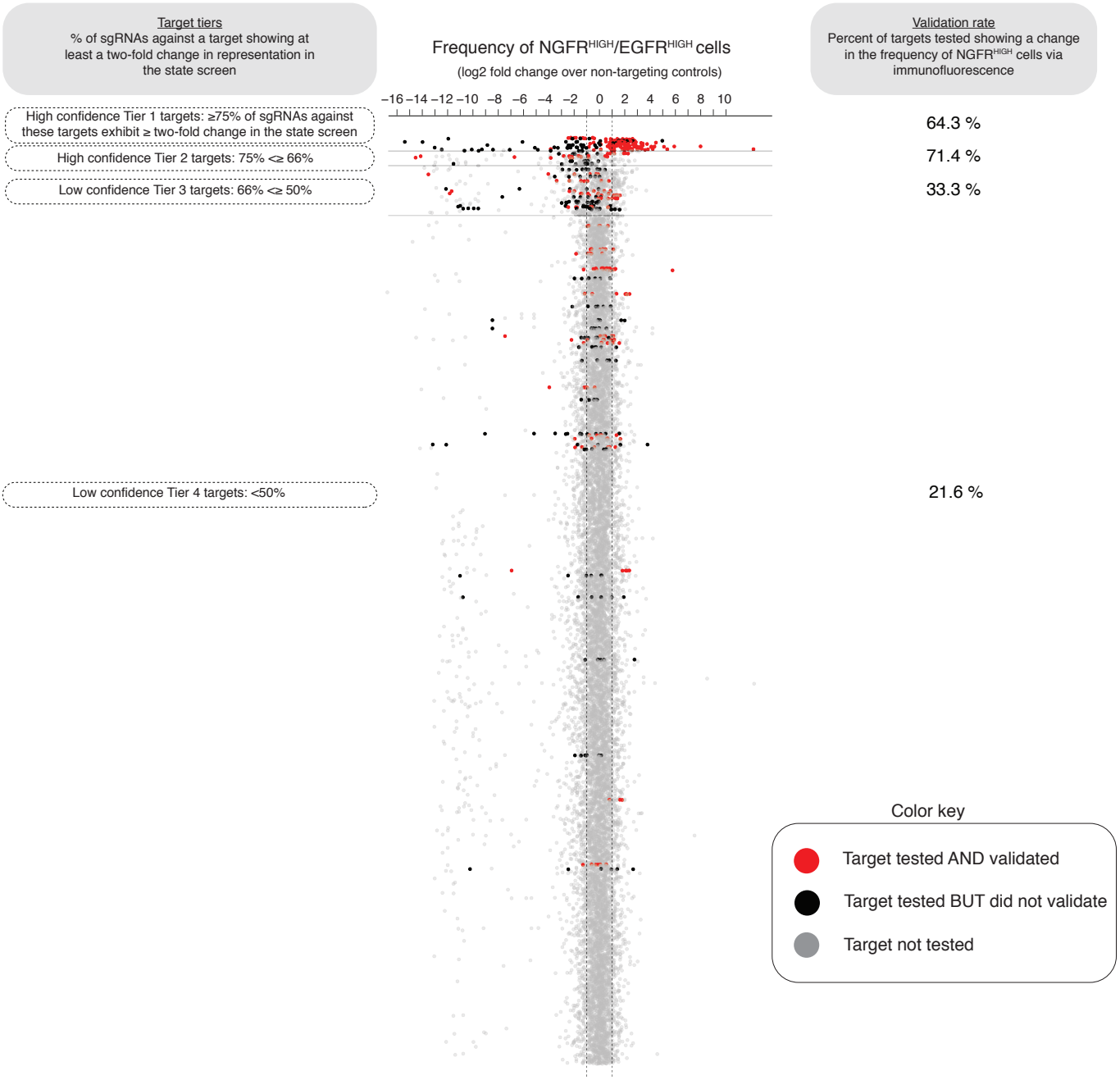

Supplemental Figure 8. Percent of targets from the state screen that validate. To assess the sensitivity of our screen, we validated the effect observed in the initial state screen for a select group of targets via NGFR immunofluorescence. Here, each dot represents an individual single guide RNA, and we plot the change in single guide RNA representation between NGFR$^{HIGH/}$EGFR^{HIGH} cells and controls (as measured in the initial state screen). We then organize all sgRNAs into tiers (y-axis, tiers one through four) based on the percent of single guide RNAs against a target showing at least a two-fold change in representation on NGFR^{HIGH}/EGFR^{HIGH} cells. In red, we labeled targets that when tested again produced at least a 50% change in the frequency of NGFR^{HIGH} cells. In black, we labeled targets that we tested but did not validate, and in gray we show targets we did not test. We displayed the percent of genes tested and validated at each tier on the right.

Supplemental Figure 9

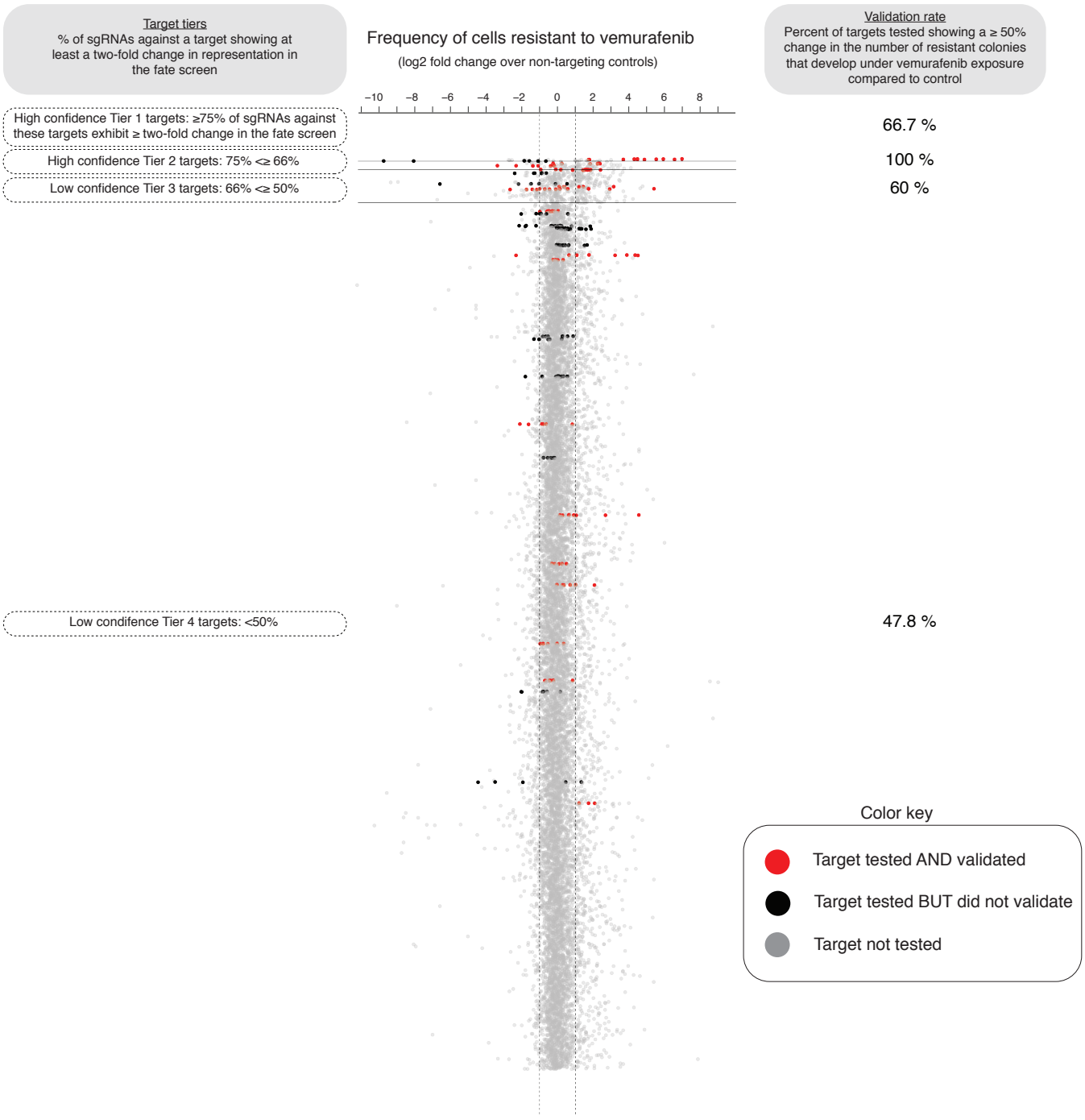

Supplemental Figure 9. Percent of targets from the fate screen that validate. To assess the sensitivity of our screen, we validated the effect observed in the initial fate screen for a select group of targets via colony formation assays. Here, each dot represents an individual single guide RNA, and we plot the change in single guide RNA representation between cells resistant to vemurafenib and cells that have never been exposed to the drug (as measured in the initial fate screen). We then organize all single guide RNAs into tiers (y-axis, tiers one through four) based on the percent of single guide RNAs against a target showing at least a two-fold change in representation on drug resistant cells. In red, we labeled targets that when tested again produced at least a 50% change in the frequency colonies resistant to $BRAF^{V600E}$ inhibition. In black, we labeled targets that we tested but did not validate, and in gray we show targets we did not test. We displayed the percent of genes tested and validated at each tier on the right.

Supplemental Figure 10

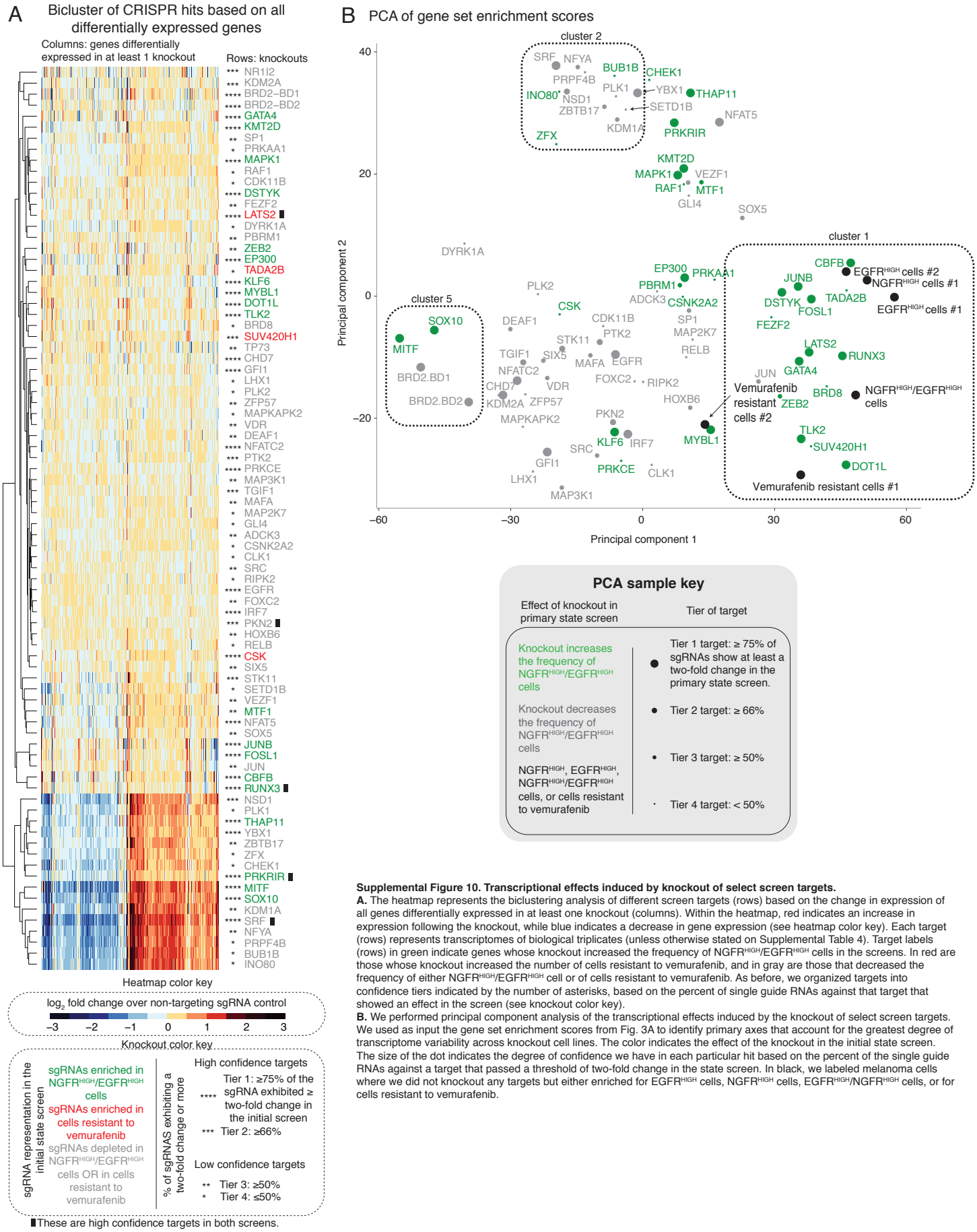

Supplemental Figure 10. Transcriptional effects induced by knockout of select screen targets.
A. The heatmap represents the biclustering analysis of different screen targets (rows) based on the change in expression of all genes differentially expressed in at least one knockout (columns). Within the heatmap, red indicates an increase in expression following the knockout, while blue indicates a decrease in gene expression (see heatmap color key). Each target (rows) represents transcriptomes of biological triplicates (unless otherwise stated on Supplemental Table 4). Target labels (rows) in green indicate genes whose knockout increased the frequency of NGFR^{HIGH}/EGFR^{HIGH} cells in the screens. In red are those whose knockout increased the number of cells resistant to vemurafenib, and in gray are those that decreased the frequency of either NGFR^{HIGH}/EGFR^{HIGH} cell or of cells resistant to vemurafenib. As before, we organized targets into confidence tiers indicated by the number of asterisks, based on the percent of single guide RNAs against that target that showed an effect in the screen (see knockout color key).
B. We performed principal component analysis of the transcriptional effects induced by the knockout of select screen targets. We used as input the gene set enrichment scores from Fig. 3A to identify primary axes that account for the greatest degree of transcriptome variability across knockout cell lines. The color indicates the effect of the knockout in the initial state screen. The size of the dot indicates the degree of confidence we have in each particular hit based on the percent of the single guide RNAs against a target that passed a threshold of two-fold change in the state screen. In black, we labeled melanoma cells where we did not knockout any targets but either enriched for EGFR^{HIGH} cells, NGFR^{HIGH} cells, EGFR^{HIGH}/NGFR^{HIGH} cells, or for cells resistant to vemurafenib.

Supplemental Figure 11

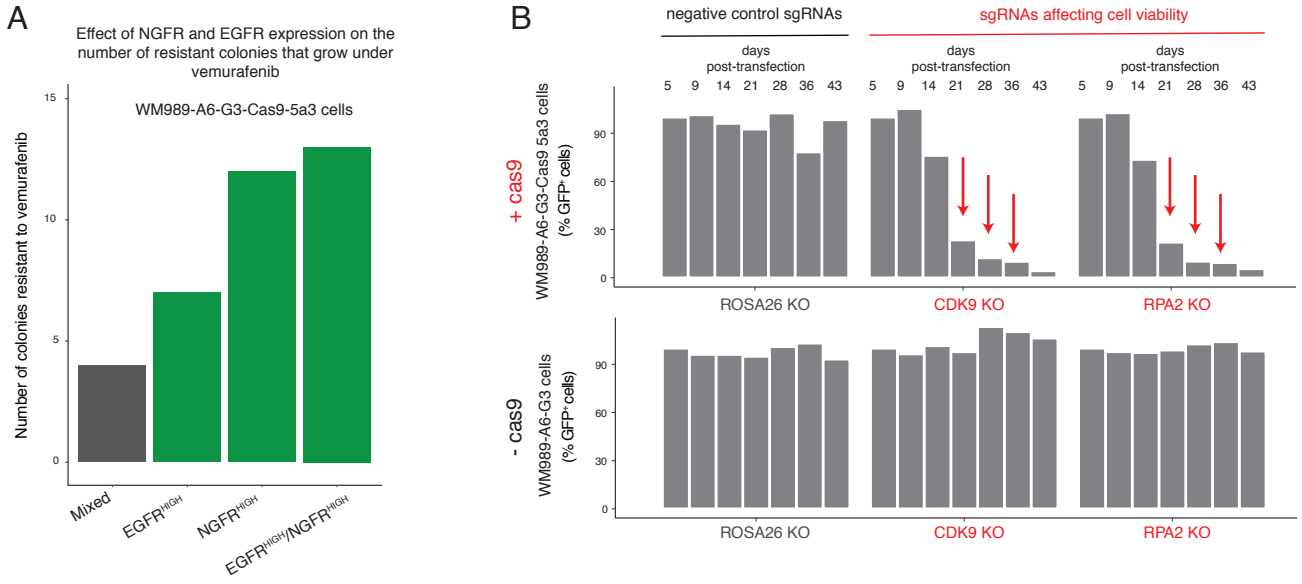

Supplemental Figure 11. Technical validation of WM989-A6-G3-Cas9-5a3 cell line.
A. WM989-A6-G3-Cas9-5a3 cells expressing NGFR, EGFR, and both NGFR and EGFR are more likely to survive and proliferate in the presence of vemurafenib (Shaffer et al. 2017). Here, we show the number of colonies that grow upon vemurafenib exposure in a mixed population of WM989-A6-G3-Cas9-5a3 or in the same population but enriched for $EGFR^{HIGH}$ cells, $NGFR^{HIGH}$ cells, or $NGFR^{HIGH}/EGFR^{HIGH}$ cells.
B. In this plot, we show the single guide RNA representation (as percent GFP-positive cells) of controls over time in WM989-A6-G3 cells with or without Cas9 expression. Negative controls (black) are single guide RNAs aimed at ROSA26, a non-expressing gene in human melanoma. Positive controls (red) target proteins necessary for cell viability. Only cells expressing both Cas9 and a positive control single guide RNA should disappear from the population over time.